

Highlights

Estimation of parameters for solar cells with S-shaped current–voltage characteristics using meta-heuristic algorithms

Oleg Olikh

- Proposed deep learning-based method to predict iron contamination in Si-SC by using IV curve.
- The simulated IV characteristics are used to create training and test datasets.
- The DNN's configurations are proposed.
- The mean squared relative error of prediction is up to 0.005.

Estimation of parameters for solar cells with S-shaped current–voltage characteristics using meta-heuristic algorithms

Oleg Olikh

Taras Shevchenko National University of Kyiv, 64/13, Volodymyrska Street, Kyiv, 01601, Ukraine

ARTICLE INFO

Keywords:
S-shaped current–voltage characteristics
Opposed two-diode model
Parameter estimation
Meta-heuristic algorithms
Nonparametric statistical procedure
Solar cell models

ABSTRACT

Defect-assisted recombination processes frequently limit the photovoltaic device performance. The low-cost and express methods of impurity contamination control are in demand at solar cell manufacturing. In this paper, we applied deep learning-based approach to extract the iron concentration in silicon solar cell from an ideality factor values.

1. Introduction

Photovoltaics (PV) is widely regarded as the most promising sustainable clean energy technology to meet the rising energy demand of our global population. By the end of 2021, the installed capacity of global solar PV panels reached an impressive 971 GW, with an additional 183 GW added in 2021 alone [1]. According to the International Energy Agency (IEA) reports, the cumulative installed PV capacity was predicted to increase to 1.826 TW by 2026 and 14.5 TW by 2050 [2]. Currently, silicon solar cells make up approximately 90% of the global photovoltaic production capacity. But recently, intensive research is underway for innovative developments, further experiments, and practical PV applications of various new-generation solar cells (SCs). The operating principle of new-generation solar cells is qualitatively similar to silicon-based ones. However, it is important to note that the fourth quadrant of their current–voltage (IV) characteristics often exhibits an S-shaped deformation or kink. This kink's origin has been attributed to various physical phenomena: charge trapping at the cathode interface [3, 4], rectifying Schottky junction at the anode interface [5] change of the electric field distribution [6], presence of strong interface dipoles [7], unbalanced charge transport [8]. Furthermore, it is worth noting that such a feature of the IV characteristics is typical in the most promising candidates for the next generation of photovoltaic devices. Specifically, S-shaped IV curves have been observed in silicon heterojunction SCs [9], thin-film SCs such as CdTe, CI(G)S, and amorphous silicon PV devices [9, 10], normal and inverted organic SCs [11, 12, 13], perovskite SCs [9, 14], quantum dot SCs [8, 15], and hybrid SCs [16, 7, 4].

One of the most common approaches to understanding the electrical characteristics of PV devices is to use an equivalent circuit model to fit the shape of the IV curve. Such lumped-parameter modeling allows simulation, analysis, and optimization of device performance. The most frequently used conventional solar cell lumped-parameter models are single-diode model (SDM), double-diode model (DDM), and three-diode model (TDM) models. The models incorporate parallel-connected diodes that activate in one

direction, a photo-current source, a parallel shunt resistance, and a series resistance. The PV module model (PVMM) is based on SDM and is made up of several diodes in series or parallel.

Unfortunately, the conventional models failed in describing the S-shaped kink. Thus, new models are proposed to give some reasonable IV curve shape explanations on the IV curve shape from the view of electricity. One of the earliest attempts to develop such a model was proposed by Mazhari [17]. This model is essentially a simplified version of the SDM, achieved by excluding resistances and incorporating an additional diode. Up to now, Mazhari's model is the simplest circuit because the least fitting parameters are required for simulations. Mazhari's model fails to capture the linear-like rise S-shaped kink in the third quadrant, and the model, which improved by incorporating two resistance, proposed for organic SCs [18]. Gaur and Kumar [11] proposed equivalent circuit models to represent the behavior of polymer solar in the dark. This model is almost identical to the DDM, except one of the diodes is the opposite. Another way to develop equivalent models involved using multiple series diodes, unlike conventional approaches. Zuo *et al.* [5] offered to explain the S-shape by utilizing a model consisting of two series diodes connected in the same direction, two shunt resistors, and one series resistor. Another lumped-parameter equivalent circuit holds two opposed diodes, two opposed current sources, and no resistors [8]. De Castro et al [6] proposed a model consisting of two opposed diodes with shunt resistance for each, a series resistance, and a photo-current source. The last model represents a significant advancement as it successfully reproduces the S-shaped kink in the power-producing fourth quadrant of the illuminated IV characteristics. However, it falls short of adequately describing the IV curve beyond the open-circuit point in the first quadrant, where the current of many practical devices tends to continue increasing [19]. To address this challenge, a potential solution was suggested — incorporating a third diode that would either replace one of the shunt resistances [20] or be placed in parallel with it [21, 10]. In general, the developing models to describe S-shaped IV curves continues. For instance, a relatively recent proposal [3] is the B2BDM model: back-to-back diodes in

 olegolikh@knu.ua (Oleg Olikh)
ORCID(s):

parallel with a shunt resistor and the photo-current source, all in series with an offset voltage source, and then connected in parallel to another diode and shunt resistor, again in series with a resistor. Some review about models for PV devices with S-shaped IV curves can be found in [19, 22].

The next step after developing the model is to identify the corresponding parameters from the IV characteristics. Essentially, this task is an optimization problem. One popular approach for solving such problems is the application of meta-heuristic algorithms. In fact, there have been numerous meta-heuristic algorithms developed specifically for this purpose. The No Free Lunch theory (NFL) [23] provides the foundation for such diversity, stating that no single meta-heuristic algorithm can solve all optimization tasks effectively. In other words, the optimization algorithm can have brilliant results in a specific class of problems and at the same time fails to solve other ones. As a result, each problem, including the parameter estimation of each equivalent model, necessitates a distinct algorithm selection. Numerous studies have been conducted to compare the efficiency of meta-heuristic algorithms for parameter estimation under conventional SC models. Some studies focus on a single model, such as SDM [24], DDM [25, 26], or TDM [27], while others examine both SDM and DDM concurrently [28, 29, 30, 31]. Several papers have investigated algorithms' efficiency in processing IV curves according to three models: SDM, DDM, and PVMM [32, 33, 34, 35, 36]. Indeed, the utilization of conventional SC models for testing newly developed algorithms is among the most popular approaches after using CEC20XX test functions. The wide range of metaheuristic optimization methods allows for situations in which various studies examine identical models but prioritize different algorithms array.

2. Problem definition

2.1. Solar cell model

Fig. 1 vividly reveals the structure of the used model [6]. It can be seen from the figure that model contains a current source accompanied by a diode D1, a shunt resistor R_{p1} to show the leakage current, and a series resistor R_s to consider the losses associated with the load current. Besides, the second diode D2 with a second parallel resistance R_{p2} is placed opposite to the first one and is essential to simulate the non-ideal effects of the active layer/cathode interface. In this model, D1 is responsible for the exponential behavior of the IV curve, the main contribution of D2 is to simulate the S-shape. The analytical solution $V(I)$ of the opposed two-diode equivalent circuit model was obtained [37] using Lambert W -function [38]:

$$\begin{aligned} V = & (I + I_{ph} + I_{01})R_{p1} \\ & - \frac{n_1 kT}{q} W \left\{ \frac{q I_{01} R_{p1}}{n_1 kT} \exp \left[\frac{q R_{p1} (I + I_{ph} + I_{01})}{n_1 kT} \right] \right\} \\ & + \frac{n_2 kT}{q} W \left\{ \frac{q I_{02} R_{p2}}{n_2 kT} \exp \left[- \frac{q R_{p2} (I - I_{02})}{n_2 kT} \right] \right\} \end{aligned}$$

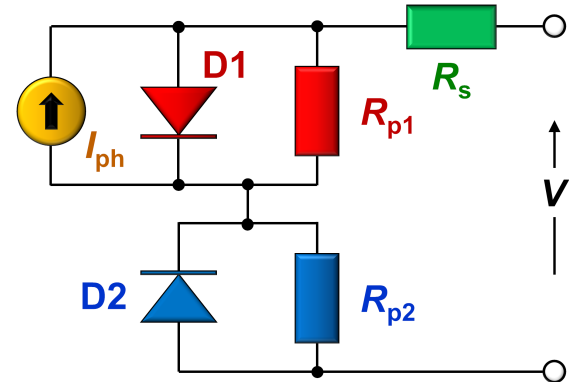


Figure 1: The opposed two-diode equivalent-circuit model of a solar cell.

$$+ (I - I_{02})R_{p2} + IR_s, \quad (1)$$

where I_{01} and I_{02} are the saturation currents and n_1 and n_2 are the ideality factors for D1 and D2 respectively, and I_{ph} is the ideal photocurrent. Thus, the model employs eight lumped parameters (I_{01} , n_1 , R_{p1} , I_{02} , n_2 , R_{p2} , R_s , and I_{ph}) that need to be determined from the IV curve. Thus, from an optimization perspective, the dimension of the problem is $D = 8$.

The expression (1) has a drawback in that it tends to stray from the range of numbers that can be accommodated by the standard 64-bit floating-point format owing to the presence of exponential functions for larger numbers. To overcome this drawback, the use of the g -function $g(x) = \ln(W(\exp(x)))$ was suggested [39]. The analytical solution $V(I)$ using the g -function is as follows [39]

$$\begin{aligned} V(I) = & IR_s + \frac{n_1 kT}{q} g(x_1) - \frac{n_2 kT}{q} g(x_2) \\ & - \frac{n_1 kT}{q} \ln \left[\frac{q I_{01} R_{p1}}{n_1 kT} \right] + \frac{n_2 kT}{q} \ln \left[\frac{q I_{02} R_{p2}}{n_2 kT} \right], \end{aligned} \quad (2)$$

with

$$x_1 = \ln \left(\frac{q I_{01} R_{p1}}{n_1 kT} \right) + \frac{q(I + I_{ph} + I_{01})R_{p1}}{n_1 kT}, \quad (3)$$

and

$$x_2 = \ln \left(\frac{q I_{02} R_{p2}}{n_2 kT} \right) - \frac{q(I - I_{02})R_{p2}}{n_2 kT}. \quad (4)$$

We used Eqs. (2)–(4) both for simulation IV curves and during the approximation procedure. The g -function was evaluated by using iterative procedure [39].

2.2. Synthetic IV curves

The research involved the parameter estimation of solar cells using meta-heuristic algorithms based on synthetic IV characteristics simulated using the opposed two-diode model. This approach allows for assessing the accuracy of the employed optimization methods, as the simulation was performed using known parameter values.

In first part of the study, a detailed analysis was conducted on a single IV curve, evaluating the performance of meta-heuristic algorithms for parameter estimation in a one-time application mainly. Additionally, the suitability of employing two different fitness functions was examined. In the second part, we simulated a set of IV characteristics and evaluated the average performance metrics of various algorithms.

2.2.1. Single-IV case

Previous studies have demonstrated [40, 41] that when the ideality factor of D2 is either equal to or significantly larger than n_1 ($n_1 = n_2 = 1.92$ or $n_1 = 1.00, n_2 = 3.00$), the nonlinear least-squares method successfully determines a set of equivalent circuit parameters that accurately replicate the experimental data of an organic photovoltaic cell. Therefore this approach does not allow for distinguishing between similar IV curves obtained from solar cells with different parameters. To overcome this issue, Tada [41] successfully employed Bayesian estimation of parameters. To assess the capabilities of meta-heuristic methods in overcoming additional similar challenges, they were applied to a IV curve corresponding to such a problematic case. The parameter values were taken from [41]:

$$\begin{aligned} I_{01} &= 1.6 \cdot 10^{-6} \text{ mA}, \\ n_1 &= 1.92, \\ R_{p1} &= 190 \Omega, \\ I_{02} &= 0.16 \text{ mA}, \\ n_2 &= 1.92, \\ R_{p2} &= 190 \Omega, \\ R_s &= 45 \Omega, \\ I_{ph} &= 8 \text{ mA}, \end{aligned} \quad (5)$$

and the IV curve was simulated over a range of 0–0.8 V with step 10 mV at $T = 300$ K. The simulation result is presented on Fig. 2 by symbols.

2.2.2. IV-set case

Employing various meta-heuristic algorithms to analyze a single IV curve is insufficient to obtain comprehensive insights into the methods' efficacy in parameter estimation. The accuracy of parameter determination is closely tied to their absolute values. For instance, an increase in the R_p value can pose challenges for accurately estimating resistance because the shunt will have a lesser impact on the overall shape of IV curve. In addition, the ratio between the parameter values also plays a crucial role.

To test the methods across different parameter values, we generated synthetic data in a temperature range from 260 K to 350 K. During the simulation process, we considered various temperature dependencies of the parameters. We based our approach on known physical mechanisms but focused on achieving the diversity of parameter ratio instead of attempting to replicate real-life photovoltaic converters precisely. Furthermore, an S-shaped IV curve is observed

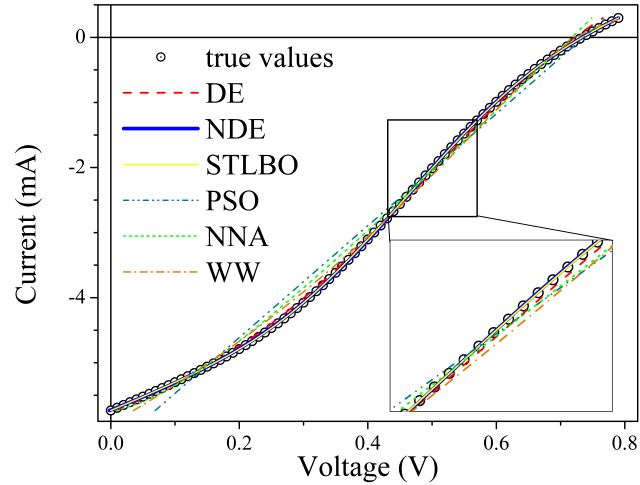


Figure 2: Fitting results (lines) for the simulated current-voltage characteristic (symbols). The values from Eq. (5) were assumed under simulation.

in solar cells of various types, and diverse charge transport mechanisms significantly complicate the selection of the only possible temperature dependence for each of the eight model parameters. Therefore, we assumed that the current conduction mechanism through D1 is close to tunneling, and hence, I_{01} , R_{p1} , and $(n_1 kT)$ remain constant, with $I_{01} = 0.015$ mA, $R_{p1} = 10^4$ Ω, $n_1 kT = 7$ eV. In the case of D2, the thermionic emission current was suggested and I_{02} and n_2 increased and decreased, respectively, with temperature rise [42]:

$$I_{02} = I_{002} \exp\left(-\frac{E_I}{kT}\right), \quad (6)$$

$$n_2 = 1 + \frac{T^*}{T}, \quad (7)$$

where I_{002} , E_I , and T^* are the constants which are independent of temperature. The values of $I_{002} = 500$ A, $E_I = 0.40$ eV, and $T^* = 500$ K were used. For R_{p2} , an exponential temperature dependence was employed, as it is widely observed [43] in modern solar cells for the shunt resistance:

$$R_{p2} = R_{p20} \exp\left(\frac{E_R}{kT}\right). \quad (8)$$

with $R_{p20} = 9$ mΩ, $E_R = 0.32$ eV. The linear temperature dependencies is expected for both I_{ph} [44, 45] and R_s [46, 47]:

$$y = y_0[1 + TC_y(T - 300)], \quad (9)$$

where $y = I_{ph}$ or R_s , y_0 is the parameter value at room temperature, TC_y is the temperature coefficient of parameter. For most types of monocrystalline silicon solar cells, the $TC_{I_{ph}}$ typically ranges from around -0.0004 K $^{-1}$ [48]. However, as the base thickness decreases, the temperature coefficient can increase to -0.0014 K $^{-1}$ [49]. For hydrogenated amorphous

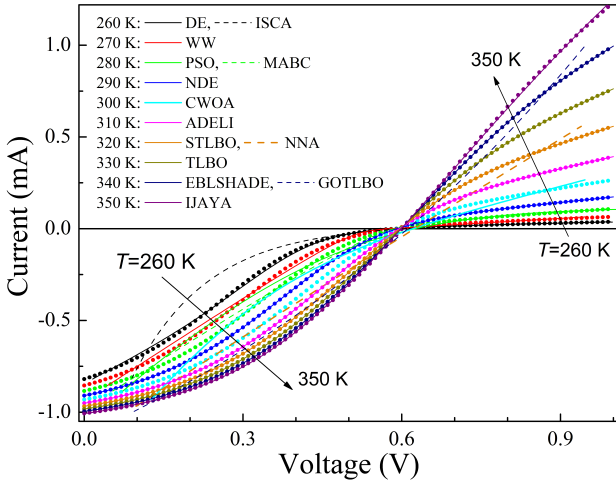


Figure 3: Fitting results (lines) for the simulated current-voltage characteristic (symbols). The values from Sec. 2.2.2 were assumed under simulation.

silicon solar cells, $TC_{I_{ph}}$ is equal to -10^{-3} K^{-1} [50]. For organic solar cells, the temperature coefficient can reach a magnitude of -0.003 K^{-1} [51]. During the simulation, we assumed $TC_{I_{ph}} = -10^{-3} \text{ K}^{-1}$. Furthermore, the values of $I_{ph0} = 1 \text{ mA}$, $TC_{R_s} = 0.02 \text{ K}^{-1}$, and $R_{s0} = 50 \Omega$ were used.

The set of I-V data was composed of 10 curves, which were simulated at 10 K intervals from 260 to 350 K; in this case, n_1 , I_{02} , n_2 , R_{p2} , R_s , and I_{ph} varied from 6.37 to 4.73, from 9 to 880 μA , from 2.92 to 2.43, from $1.4 \cdot 10^4$ to 360 Ω , from 10 to 100 Ω , and from 0.96 to 1.05 mA, respectively. The simulation results are presented on Fig. 3 by symbols.

2.3. Meta-heuristic algorithms

In the literature, meta-heuristics are frequently categorized based on their sources of inspiration. This categorization involves incorporating elements of true simulations and principles that incorporate stochasticity, with the objective of emulating diverse characteristics observed in biological behavior, the lives of creatures in nature, human behavior, or natural phenomena. On this basis, any meta-heuristic algorithm can fall into one of the following main classes [52, 53, 54]: evolution-based methods (emulate the principles of evolutionary behavior observed in creatures in nature by relying on the concept of survival of the fittest), swarm intelligence-based methods (simulate the collective, dynamic, intelligent, and concerted gregarious conduct of collections of flocks or communities found in nature), bio-based methods (use biological processes unrelated to group behavior), chemical & physical-based methods (originate from the physical phenomena or chemical laws that exist in the universe), human-society-based methods (inspired by human beings, including various activities such as thinking and social behavior), and math-based methods (borrow the mathematical functions). Generally, there are hundreds of meta-heuristic optimization methods available. While we

acknowledge that our selection may not be fully comprehensive, we utilized 14 methods, representing all classes mentioned above, to tackle the parameter estimation task within the framework of the opposed two-diode model for a solar cell. Hereafter, we provide a succinct description of each method alongside the parameters employed during the fitting process.

Differential evolution (DE). DE is one of the classical methods, and it is based on the natural selection law and uses the randomly generated initial population, differential mutation, and probability crossover [55]. During the implementation, we employed a penalty function suggested by Ishaque *et al* [56]. Besides, according to Wang and Ye [55], the values of mutation scaling factor $F = 0.8$, crossover rate $Cr = 0.3$, and population size $Np = 8 \times D = 64$ were used in this work.

Adaptive differential evolution with the Lagrange interpolation argument (ADELI). The method is based on DE, which integrates an adaptive local search scheme with Lagrange interpolation [57]. This incorporation aims to enhance the exploitation capability and accelerate the convergence speed. In ADELI, the scaling factor and crossover rate are set to self-adapting to optimize the results. We used parameter values recommended by Huang *et al* [57] during the implementation process. Additionally, we set Np to 64 for our numerical experiments.

Differential evolution with neighborhood-based adaptive evolution mechanism (NDE). The method uses a mutation strategy, which takes into account neighborhood and individual information, and an adaptive evolution mechanism [58]. The determination of F and Cr values is achieved through the utilization of the weighted adaptive procedure [59], and an adaptive adjustment of the population size is implemented using a simple reduction method (from $10 \times D = 80$ to 5).

Success history based DE with hybridization mutation strategies and population size reduction (EBL SHADE). The method is the hybridization framework between $pbest$ and ord_pbest mutation strategies and stores a set of Cr and F values that have performed well in the recent past [60]. A linear Np reduction (from $18 \times D = 144$ to 4) is used as well.

Particle swarm optimization (PSO). It is another classic method based on observations of the social behavior of animals, such as bird flocking, fish schooling, and swarm theory. According to Ye *et al.* [61], the values of learning factors $l_1 = l_2 = 2$, the final weight and the initial weight $w_{max} = 0.9$, $w_{min} = 0.4$, and $Np = 15 \times D = 120$ are used in this work.

Modified artificial bee colony (MABC) algorithm is based on the intelligent foraging behavior of honey bee swarms [62]. The control parameters include the population size ($Np = 8 \times D = 64$) and the maximum number of generations after which each non-improved food source is to be discarded ($L_{init} = 36$).

Chaotic Whale Optimization Algorithm (CWOA). WOA draws inspiration from the hunting behavior of humpback whales [63]. On the other hand, CWOA employs chaotic

maps to compute and dynamically adjust its internal parameters [64]. In our study, we utilized the Singer chaotic map and set $N_p = 100$ for the identification of the parameters of the solar cell.

The *Neural Network Algorithm (NNA)* is a meta-heuristic algorithm that draws inspiration from both biological nervous systems and artificial neural networks [65]. The recommended [65] value $N_p = 50$ is used in our paper.

The *teaching learning based optimization (TLBO)* algorithm employs the concept of passing on knowledge within a classroom. Similar to learners acquiring knowledge from a teacher and interacting with their peers, TLBO incorporates such interactions [66]. In this study, a value of $N_p = 100$ is utilized.

Generalized oppositional teaching learning based optimization (GOTLBO). This method integrates a concept that incorporates both the current estimate and its opposite estimate simultaneously into the original TLBO algorithm through the initialization step and generation jumping [67]. The values of jumping rate $Jr = 1.0$ and $N_p = 20$ were used.

Simplified teaching-learning based optimization algorithm (STLBO). In STLBO, an elite strategy is employed to improve the searching capability, and a the chaotic map is used to enrich the uniformity of random values in the mutation phase [68]. The logistic chaotic map and $N_p = 20$ were used.

Water wave optimization (WWO) takes inspiration from shallow water wave models and borrows ideas from wave propagation, refraction, and breaking [69]. WWO is easy to implement with a small-size population, and there are four control parameters: the maximum wave height h_{max} , the wavelength reduction coefficient α , the breaking coefficient β , and the maximum number k_{max} of breaking directions. According to Zheng [69], we used the values $h_{max} = 6$, $\alpha = 1.026$, $N_p = 10$, $k_{max} = \min(12, D/2) = 4$, and β linearly decreased from 0.25 to 0.001.

Improved JAYA (IJAYA). Jaya algorithm is based on the concept that the solution obtained for a given problem should move toward the best solution and should avoid the worst solution and does not require any algorithm-specific parameter [70]. In IJAYA, a self-adaptive weight is introduced to adjust the tendency of approaching the best solution and avoiding the worst solution; an experience-based learning strategy is employed to maintain the population diversity and enhance the exploration ability, and a chaotic elite learning method is proposed to refine the quality of the best solution in each generation [36]. The logistic chaotic map and $N_p = 4 \times D = 32$ were used.

Improved sine cosine algorithm (ISCA). SCA based on simulating the behaviors of sine and cosine mathematical functions [71]. ISCA implementation included a modified position-updating equation based on inertia weight ($w_{start} = 1$, $w_{end} = 1$), a nonlinear conversion parameter strategy based on the Gaussian function ($a_{start} = 2$, $a_{end} = 0$) [72], the creation of the opposite population to jump out from the local optima with $Jr = 0.1$ [73], a greedy selection, and $N_p = 30$.

The majority of the utilized algorithms demonstrate excellent performance when it comes to parameter estimation of solar cells within conventional models (single or double diode) [64, 55, 67, 36, 62, 61, 68, 66, 74, 35].

In meta-heuristic optimization methods, the quality of the extracted parameters is evaluated using the fitness function at every iteration. In our investigation, absolute error and square error fitness functions were under consideration:

$$F_{AE}(Y) = \sum_{k=1}^p \left| V^{tr}(I_k) - V^{cal}(I_k, Y) \right|, \quad (10)$$

$$F_{SE}(Y) = \sum_{k=1}^p \left[V^{tr}(I_k) - V^{cal}(I_k, Y) \right]^2, \quad (11)$$

where $V^{tr}(I_k)$ is the simulated value of voltage at current I_k , $V^{cal}(I_k, Y)$ is the calculated values of voltage, which can be obtained by Eqs. (2)–(4), for given set of parameters (i.e. $Y = \{I_{01}, n_1, R_{p1}, I_{02}, n_2, R_{p2}, R_s, I_{ph}\}$) at current I_k , and p is the total number of voltage steps in the IV characteristic.

We executed each tested algorithm for $N_{runs} = 51$ independent runs on each simulated IV curve to generate the statistical results. The search ranges were set as follows: $I_{01}(\text{mA}) \in [10^{-13}, 1]$, $n_1 \in [0.5, 50]$, $R_{p1}(\Omega) \in [10, 10^6]$, $I_{02}(\text{mA}) \in [10^{-7}, 10]$, $n_2 \in [0.5, 50]$, $R_{p2}(\Omega) \in [10, 5 \cdot 10^4]$, $R_s(\Omega) \in [0.1, 1000]$, $I_{ph}(\text{mA}) \in [10^{-3}, 100]$.

2.4. Evaluation metrics

To better show the performance differences between compared algorithms, several evaluation metrics are considered, which can be described as follows:

1. Mean value (MEAN), median value (MEDIAN), standard deviance (STD), and interquartile range (IQR) for each two-diode model parameter y (y is one of $\{I_{01}, n_1, R_{p1}, I_{02}, n_2, R_{p2}, R_s, I_{ph}\}$). MEAN and MEDIAN are often used to measure the solution quality. The closer the obtained MEAN and MEDIAN values are to the actual parameter values, the closer the obtained solution is to the optimal solution. To quantify, we used the absolute percentage of error (APE):

$$APE(y) = \left| \frac{y - y^{tr}}{y^{tr}} \right|, \quad (12)$$

where y^{tr} is the parameter value used during the IV curve simulation. APE was calculated for y_i , obtained by one-run algorithm application (APE_i), MEAN (APE_{MEAN}), and MEDIAN (APE_{MEDIAN}). Reducing STD and IQR result in a more stable algorithm performance.

2. Another evaluation criterion used to compare the algorithms' performance is to compare their execution time. We used average run time t_{run} in seconds for an individual optimizer on one IV curve.

3. Root mean square percentage of error (RMSPE) is a statistical measure that indicates how well the fitted curve matches the actual IV curve:

$$\text{RMSPE} = \sqrt{\frac{1}{p} \sum_{k=1}^p \left[\frac{V^{\text{tr}}(I_k) - V^{\text{cal}}(I_k, Y)}{V^{\text{tr}}(I_k)} \right]^2}. \quad (13)$$

4. Wilcoxon signed-rank test is a nonparametric statistical test used for pairwise comparisons of algorithms. This test assigns a rank to all the scores considered as one group and then sums the ranks of each group.
5. Friedman, Friedman Aligned Ranks, and Quade tests are used for comparing the performance differences among optimization algorithms (multiple comparisons $1 \times N$ with a control method). Therefore, the average rankings of the algorithms according to the tests are reported. Besides, the post-hoc Finner, Holm, Hochberg, and Holland procedures are used to establish proper comparisons between each algorithm and a set of other algorithms.
6. Multiple Comparisons Test (Friedman) with Shaffer's static, Nemenyi, and Holm procedures are employed to compute all possible pairwise comparisons between groups ($N \times N$) and identify the differences.

3. Numerical results and discussion

3.1. Comparison of algorithms time

In meta-heuristic algorithms, a different termination can be defined. For instance, a termination condition can be a specific number of iterations N_{it} , constraints on the number of fitness function evaluations N_{FE} , a specific rate of precision, a specific time, no sign of change in solutions after a specific number of iterations, or a combination of these cases [75]. In this study, the primary focus was on the accuracy of parameter estimation. Therefore to ensure that both exploration and exploitation processes could be fully realized by each algorithm with an equal opportunity, the termination criterion used was the absence of changes in the solution. Based on this condition, the required number of iterations N_{it} was determined, and the corresponding calculation time was measured t_{run} . In addition, the N_{FE} was evaluated.

All the applied algorithms have been coded and implemented in Embarcadero®Delphi 10.3 programming software. The run time was estimated by using WinAPI-functions *QueryPerformanceCounter()* and *QueryPerformanceFrequency()*. The experiments were performed on Windows 10 Pro 64-bit, 2.9 GHz AMD Ryzen 7 4800H CPU, and 8 GB RAM.

The obtained results are listed in Table 1. As can be seen from the table, the number of iterations required for an algorithm does not always correlate directly with the number of fitness function evaluations or computation time needed to converge. The reason is the unique features of each algorithm. The run time of the algorithms varies considerably, with a range of 1.5 seconds to 93 seconds. Notably, WW, ISCA, NNA, and STLBO converge the fastest, while ADELI, TLBO, and MABC require the most time.

Table 1

Comparison of optimization algorithms for single IV curve parameter estimation

Algorithm	N_{it}	N_{FE}	$t_{\text{run}} (\text{s})$
DE	8000	1024000	42 ± 1
EBSL SHADE	3000	444600	22 ± 1
ADELI	12000	1800000	93 ± 2
NDE	5000	430000	20.2 ± 0.3
MABC	8000	1024000	48 ± 11
TLBO	5000	1000000	56.1 ± 0.3
GOTLBO	6000	360000	15 ± 1
STLBO	13000	273000	13.8 ± 0.3
PSO	4000	480000	19 ± 3
IJAYA	30000	960000	37 ± 1
ISCA	5000	150000	6.5 ± 0.1
NNA	5000	250000	10.6 ± 0.5
CWOA	3000	300000	16.6 ± 0.5
WW	3000	35000	1.4 ± 0.1

Table 2

Wilcoxon signed ranks test results of fitness functions comparisons with a level of significance $\alpha = 0.05$

Algorithm	Parameter								
	I_{01}	n_1	R_{p1}	I_{02}	n_2	R_{p2}	R_s	I_{ph}	RMSPE
DE	SE	SE	=	=	SE	SE	=	=	=
EBSL SHADE	SE	=	=	=	=	=	=	=	AE
ADELI	SE	=	=	=	=	=	=	=	AE
NDE	=	=	=	=	=	=	=	SE	SE
MABC	=	SE	=	=	=	=	=	=	SE
TLBO	SE	SE	SE	SE	SE	SE	SE	SE	SE
GOTLBO	=	=	=	=	SE	=	=	=	
STLBO	SE	=	=	=	=	=	=	=	AE
PSO	=	=	=	=	=	AE	=	=	
IJAYA	AE	AE	=	=	SE	=	=	=	=
ISCA	=	=	=	=	=	=	=	=	=
NNA	=	=	=	=	=	=	=	=	SE
CWOA	=	=	SE	=	AE	=	=	=	SE
WW	=	=	SE	=	AE	=	=	=	SE

3.2. Fitness function selection

To choose the more suitable fitness function, we evaluated each algorithm using the IV curve generated from the parameters provided in Eq. (5) with both F_{AE} and F_{SE} functions (see Eqs. (10) and (11)). Afterward, the results obtained using each of the functions were compared through pairwise comparisons. In this case, the absolute percentage error values obtained for one-run algorithm application (APE_i) were used. Table 2 gives the statistical results produced by Wilcoxon sign-rank test with a significant level $\alpha = 0.05$. A cell marked with the symbol “SE” indicates that estimation of parameter specified in the column by the algorithm with F_{SE} outperforms result obtained by this algorithm with F_{AE} . A cell marked with the symbol “AE” indicates better results for function F_{AE} . In the case of the symbol “=”, there is no significant difference between function F_{SE} and function F_{AE} application.

As evidenced in the provided data, utilizing the square error fitness function more frequently yields better outcomes in comparison to F_{AE} . In rare cases, the absolute error fitness function can enhance the alignment between the fitted and actual curves, as well as improve the accuracy of some parameter estimations by PSO, IJAVA, CWOA, and WW algorithms. However, RMSPE is not the most crucial factor in determining model parameters, and the mentioned methods, as will be shown later, do not provide the highest accuracy. As such, the results presented in the following sections are exclusive to the application of the F_{SE} function. Therefore, it can be recommended that researchers consider the square error fitness function as a more effective and reliable option for the task of opposed two-diode model parameter estimation.

3.3. Performance comparison

3.3.1. Evaluation of single-IV

In this subsection, we show and analyze the statistical results of different meta-heuristic algorithm applications to an IV curve, simulated with Eq. (5) values. Several typical fitting results of the synthesized curve are shown in Fig. 2. A more comprehensive version, including the fitting results obtained using each algorithm, is provided in the supplementary materials (figure S1). It can be seen, that the closest match between the approximation curves and the IV curve points is observed for EBL SHADE, ADELI, NDE, IJAYA, TLBO, and STLBO. On the contrary, the PSO and GOTLBO fitting curves had the least replication of the original data.

Fig. 4 shows the results of cell parameters estimation by comparative algorithms. In addition, the figure presents the RMSPE data, which confirms the conclusions of the visual comparison between the fitting lines and the points of the IV curve. The results in terms of MEAN, MEDIAN, STD, and IQR are tabulated as well (table S1 in the supplementary material).

We would like to stress the following. In most cases, median values are more relevant to the actual parameter values than the mean values. Possible exceptions only apply to the estimation of R_s and R_{p2} only. However, in cases where a method allows for parameter estimation with high accuracy (EBL SHADE, ADELI, TLBO, and STLBO), MEDIANs are at least as good as the MEANS. As a result, we will utilize median values as a robust measure of central tendency in nonparametric statistical tests. Secondly, the increase in algorithm stability (reduction in STD and IQR values) in determining each model parameter correlates with the accuracy of parameter estimation. Furthermore, IQR values are generally no worse than STD values. Finally, small RMSPE values (close match between the fitting curve and the IV points) do not always indicate high accuracy in determining the parameters of a solar cell — see IJAYA and NDE data. For example, the difference between the MEDIAN_{RMSPE} values for NDE and ADELI is approximately 0.0001 (about 0.08% of their absolute value). At the same time, in the ADELI case, the values of APE_{MEDIAN} do not exceed $6 \cdot 10^{-4}$ for all model parameters estimation,

whereas for the NDE algorithm application, the obtained APE_{MEDIAN} values are significantly higher and range from 0.04 for I_{ph} to 11.4 for I_{01} . On one hand, this confirms the issue identified by Tada [40, 41], which arises when estimating parameters according to the opposed two-diode model from similar IV curves corresponding to photovoltaic cells with distinct characteristics. Furthermore, the results indicate that some metaheuristic algorithms, such as NDE and IJAYA, can fall into a similar trap. On the other hand, the high accuracy in parameter estimation demonstrated by EBL SHADE, ADELI, and STLBO indicates that these algorithms are able to overcome the mentioned issue when applied. It should be noted that a similar problem has been previously addressed by employing Bayesian estimation of parameters [41]. However, each Bayesian calculation took approximately half a day on a computer better equipped than ours [41]. In our case, when applying meta-heuristic algorithms, the worst-case run time did not exceed 100 seconds.

In order to statistically compare the algorithm under consideration, we use nonparametric tests. In the single-IV case, all nonparametric statistical tests were used to compare the performance of meta-heuristic algorithms in assessing each of the eight model parameters. The APE_i values were used, and the number of case problems in the study N_{pr} was equal to $N_{runs} = 51$. Additionally, algorithms were compared in terms of curve-fitting accuracy by using RMSPE values. Furthermore, tests were employed for a composite parameter as well. This parameter, referred to as “Comp” hereafter, includes APE_{MEDIAN} for each of the eight defined model parameters, the median value for RMSPE, and t_{run} . This parameter may provide the most valuable insights for comparing algorithms. However, it is important to note that the value of N_{pr} is only 10. According to Derrac *et al* [76], the number of case problems should be $N_{pr} \geq 2k$, where k is the number of algorithms ($k = 14$ in our study). Therefore, the use of the Comp parameter is not strictly rigorous. Indeed, it would have been possible to increase the N_{pr} value using, for example, APE_{MEAN}. However, considering the deliberate utilization of a suboptimal parameter would have appeared inappropriate.

Fig. 5 graphically show the non-parametric statistical results of pairwise comparisons of algorithms based on the Wilcoxon signed-rank test. In the case of Comp comparisons, the differences in performance scores were normalized to the interval [0, 1]. As seen from the figure, no algorithm outperforms all others in evaluating each parameter. Furthermore, no algorithm surpasses all others in the estimation even a single parameter. For example, as the figure states, STLBO shows a significant improvement over DE, NDE, MABC, GOTLBO, PSO, IJAYA, ISCA, NNA, CWOA, and WW across all the parameters considered with a level of significance $\alpha = 0.05$. Simultaneously, it was not detected the significant differences between STLBO and both EBL SHADE and ADELI for all parameter estimations as well as between STLBO and TLBO in the Comp case. EBL SHADE outperforms nearly all other algorithms in the

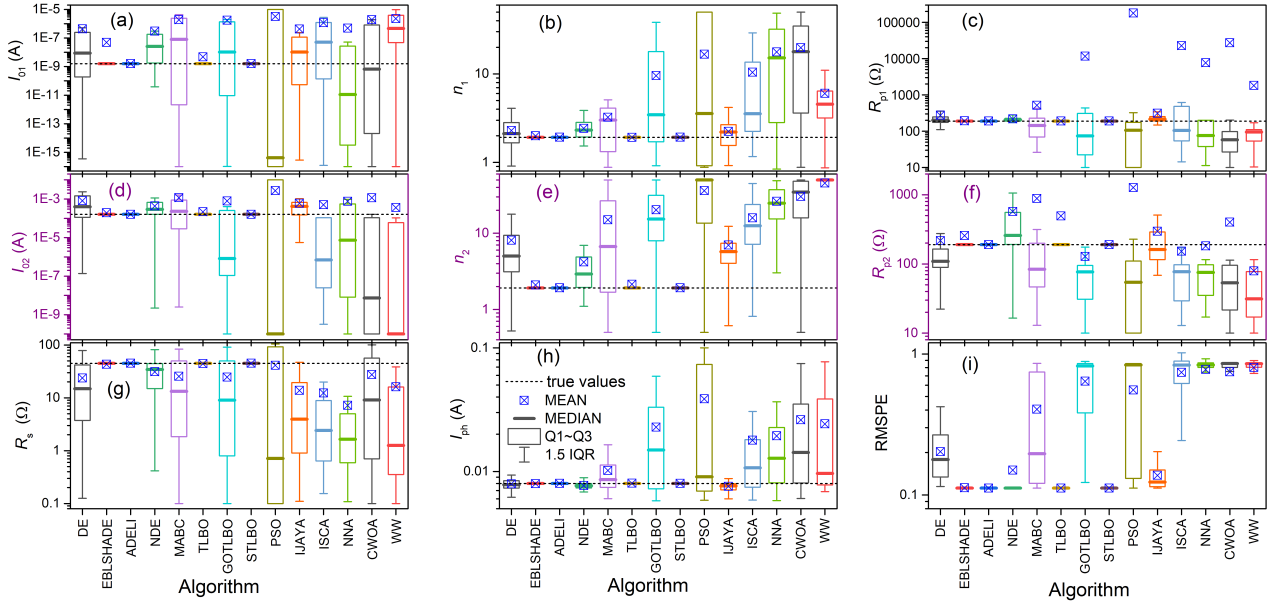


Figure 4: Box-plot of two-diode model parameter estimation from single IV curve using different optimizers. The squares are the mean values, and the dashed lines correspond to the true parameter values.

composite parameter, except for STLBO. According to the Wilcoxon test victories count, the worst performances are exhibited by PSO and CWOA. PSO achieved better results than ISCA, NNA, and CWOA in terms of RMSPE value, as well as outperformed WW in n_2 estimation and RMSPE. Test detected significant differences between CWOA and WW in n_2 and I_{01} estimations, between CWOA and PSO in I_{01} , I_{02} , R_s , and I_{ph} estimations, and between CWOA and both ISCA and NNA in R_s estimation case only.

Looking at the results of the Wilcoxon signed-rank test from another perspective, it can be observed that neither EBL SHADE nor STLBO had any defeats in pairwise comparisons, while ADELI had only one loss. ADELI was only outperformed by EBL SHADE in terms of the Comp parameter, primarily due to its significantly longer run time. The highest count of defeats was observed for the PSO and WW algorithms (104 and 84, respectively). The data regarding the total count of wins and losses when applying the Wilcoxon test for each algorithm are summarized in Fig. 6.

It is recommended [76] to begin the multiple comparisons tests by examining the null hypothesis H_0 , which asserts the equality of medians between the populations of results obtained by different algorithms. The null hypothesis p -values computed through the statistics of Friedman, Friedman Aligned, and Quade test and the Iman–Davenport extension are given in the supplementary material (table S2). The highest observed $p(H_0)$ -values were found to be $2.7 \cdot 10^{-5}$ (Friedman Aligned test for the task of R_{p1} estimation), $4.4 \cdot 10^{-4}$ (Friedman Aligned test for the composite parameter case), and $8.3 \cdot 10^{-6}$ (Quade test, Comp parameter). Thus obtained data strongly suggest the existence of significant differences among the considered algorithms in the accuracy of all model parameter determination, RMSPE values, and Comp parameter.

Fig. 7 shows ranks achieved by the Friedman, Friedman Aligned, and Quade tests for applied optimization algorithms in different tasks. Ranks are tabulated in the supplementary material as well (table S3). In almost all cases, the algorithms EBL SHADE, ADELI, and STLBO consistently achieve the top (smallest value) three ranks. For example, in assessing the accuracy of model parameter estimation, ADELI has ranked first 22 times. The STLBO algorithm ranked first six times, taking the sole first place twice (I_{01} estimation according Friedman Aligned test and R_{p1} estimation according Quade test) and sharing it with ADELI four times (n_1 , R_{p1} , n_2 , and I_{ph} estimation according Friedman Aligned test). In the RMSPE value case, ADELI and STLBO achieved equal and best ranks by all three used tests. When comparing based on the Comp parameter, the STLBO algorithm obtained the top rank according to the Friedman Aligned test, while the Friedman and Quade tests recognized EBL SHADE as the best. In most cases, the TLBO algorithm secured the fourth position, and in four cases, it even ranked third. In the majority of cases, the TLBO algorithm consistently ranked fourth out of all the algorithms tested. Interestingly, in four cases (I_{01} estimation, RMSPE value, and Comp parameter by Friedman Aligned test, and Comp parameter by Quade test), it even achieved a commendable third-place ranking. We must note that overall, the absolute values of ranks for ADELI, STLBO, EBL SHADE and TLBO algorithms differ little, and the difference between the first and fourth ranks is often less than 0.5. The worst ranks are observed for PSO, NNA, CWOA, and WW.

It is known [76] that the Friedman, Friedman Aligned, and Quade tests are insufficient in establishing accurate comparisons between the algorithms considered. To compare a control method (1 of 14 compared) with a set of

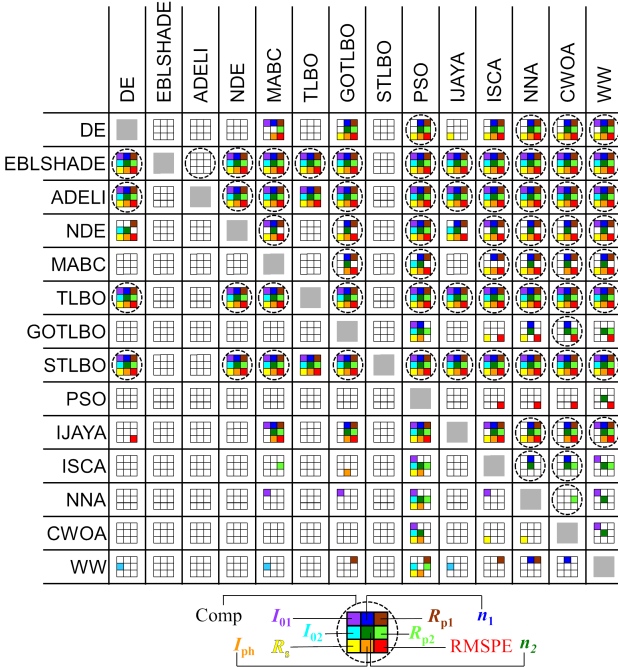


Figure 5: The results of Wilcoxon signed-rank test with a level of significance $\alpha = 0.05$ in the single-IV case. Each colored small square indicates that the algorithm specified in the row outperforms the algorithm specified in the column in evaluating one of the parameters of the two-diode model. The correspondence between the color and position of the square to a model parameter is shown in a legend at the figure bottom. The advantage of the row algorithm in the Comp parameter is indicated by the presence of a dashed circle.

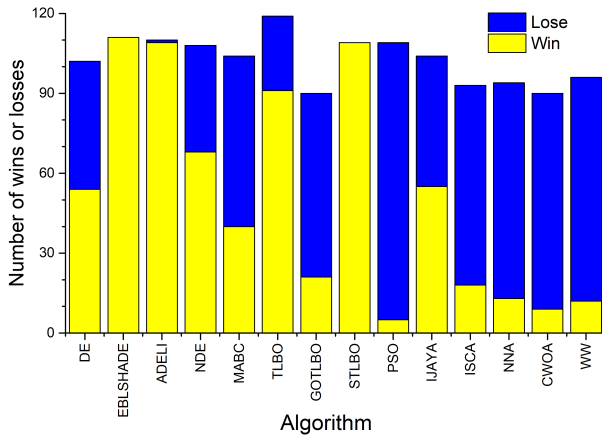


Figure 6: The total count of wins and losses for each algorithm in pairwise comparisons using the Wilcoxon signed-rank test with a significance level of $\alpha = 0.05$ in the single-IV case.

other algorithms (rest 13), one can define a family of hypotheses related to the control method. Applying a post-hoc test makes it possible to obtain a p -value that indicates the extent to which each hypothesis can be rejected. We calculated p -values using four post-hoc procedures (Finner, Holm, Hochberg, and Holland) for all algorithms, tests, and

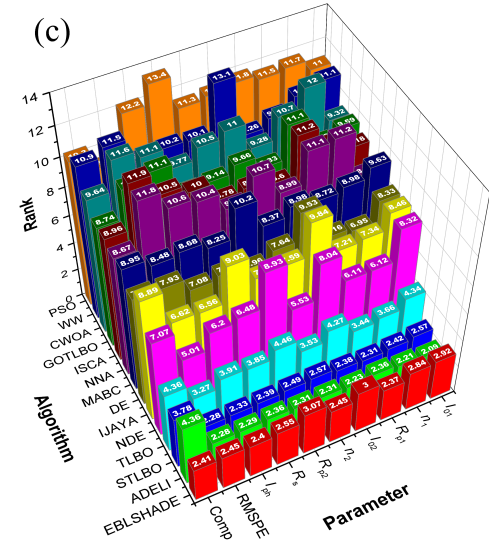
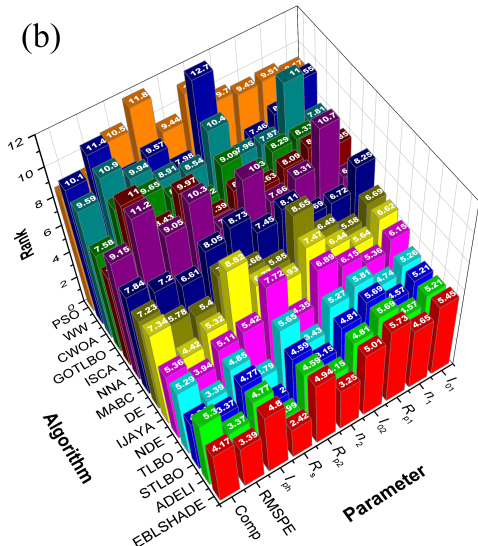
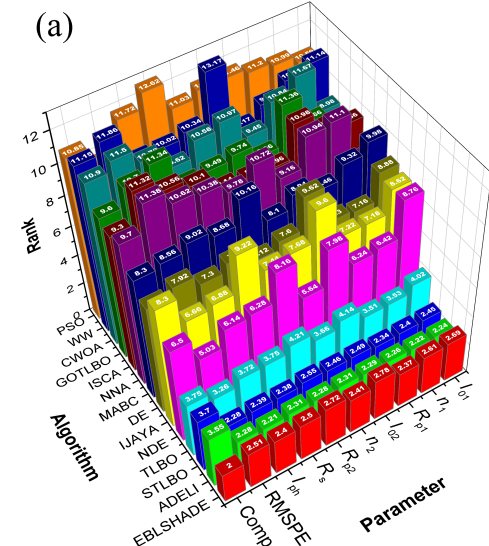


Figure 7: Ranking of the algorithms according to Friedman (a), Friedman Aligned (b), and Quade (c) tests in the single-IV case.

Table 3

Adjusted p -values for Friedman, Friedman Aligned, and Quade tests in single-IV case. ADELI is the control algorithm, and the task of R_{p1} estimation is under consideration.

Algorithm	Test	Finner	post-hoc procedure		
			Holm	Hochberg	Holland
GOTLBO	Friedman	<1E-13	<1E-13	<1E-13	<1E-13
	Friedman Aligned	2.23361E-09	6.87266E-09	6.87266E-09	6.87266E-09
	Quade	2.57827E-03	4.09880E-03	3.90245E-03	4.09117E-03
PSO	Friedman	<1E-13	<1E-13	<1E-13	<1E-13
	Friedman Aligned	<1E-13	<1E-13	<1E-13	<1E-13
	Quade	2.57827E-03	2.58134E-03	2.58134E-03	2.57827E-03
MABC	Friedman	6.35048E-13	1.61204E-12	1.61204E-12	1.61204E-12
	Friedman Aligned	7.88131E-06	2.97065E-05	2.97065E-05	2.97062E-05
	Quade	1.73550E-02	6.56791E-02	6.56791E-02	6.38590E-02
WW	Friedman	1.84926E-10	5.69003E-10	5.69003E-10	5.69003E-10
	Friedman Aligned	3.15599E-13	8.01137E-13	8.01137E-13	8.01137E-13
	Quade	5.31725E-03	1.96611E-02	1.96611E-02	1.94928E-02
DE	Friedman	4.61292E-09	1.59678E-08	1.59678E-08	1.59678E-08
	Friedman Aligned	3.62181E-04	1.33738E-03	1.33738E-03	1.33663E-03
	Quade	7.62673E-02	2.85885E-01	2.49968E-01	2.53918E-01
IJAYA	Friedman	6.88175E-09	2.54096E-08	2.54096E-08	2.54096E-08
	Friedman Aligned	8.79672E-04	3.04543E-03	3.04543E-03	3.04172E-03
	Quade	7.62673E-02	2.85885E-01	2.49968E-01	2.53918E-01
CWOA	Friedman	8.73483E-09	3.29236E-08	3.29236E-08	3.29236E-08
	Friedman Aligned	4.27917E-09	1.58000E-08	1.58000E-08	1.58000E-08
	Quade	2.57827E-03	5.93402E-03	5.93402E-03	5.91840E-03
NNA	Friedman	1.17491E-08	4.33811E-08	4.27586E-08	4.33811E-08
	Friedman Aligned	2.23361E-09	7.25937E-09	7.25937E-09	7.25937E-09
	Quade	2.57827E-03	4.09880E-03	3.90245E-03	4.09117E-03
ISCA	Friedman	1.23525E-08	4.33811E-08	4.27586E-08	4.33811E-08
	Friedman Aligned	<1E-13	<1E-13	<1E-13	<1E-13
	Quade	2.57827E-03	3.65691E-03	3.65691E-03	3.65079E-03
NDE	Friedman	2.55436E-06	7.85957E-06	7.85957E-06	7.85955E-06
	Friedman Aligned	4.19953E-02	1.29854E-01	1.29854E-01	1.23666E-01
	Quade	1.60056E-01	5.02233E-01	5.02233E-01	4.15313E-01
TLBO	Friedman	1.57702E-01	4.05499E-01	4.05499E-01	3.53159E-01
	Friedman Aligned	6.48054E-01	1.0	1.0	9.29409E-01
	Quade	7.18467E-01	1.0	1.0	9.59945E-01
EBLSHADE	Friedman	9.13338E-01	1.0	9.23824E-01	9.89059E-01
	Friedman Aligned	8.67482E-01	1.0	1.0	9.76034E-01
	Quade	9.98363E-01	1.0	1.0	9.99993E-01
STLBO	Friedman	9.23824E-01	1.0	9.23824E-01	9.89059E-01
	Friedman Aligned	1.0	1.0	1.0	1.0
	Quade	1.0	1.0	1.0	1.0

tasks. By following the indications given for the four post-hoc procedures considered, Table 3 shows the p -values obtained, using the ranks computed by the Friedman, Friedman Aligned, and Quade tests for the case of control algorithm ADELI and the task of R_{p1} estimation. These are typical results, the reader is referred to the supplementary material for rest of p -values (Tables S4-S143).

As we can see in the table, the Finner post-hoc procedure exhibits the most powerful behavior, reaching the lowest p -values in the comparisons. The Friedman test shows a significant improvement in R_{p1} estimation of ADELI over DE, NDE, MABC, GOTLBO, PSO, IJAYA, ISCA, NNA, CWOA, and WW for all the post-hoc procedures considered.

The Friedman Aligned test only confirms the improvement of ADELI over the aforementioned 10 algorithms for every post-hoc procedure considered, except Holm, Hochberg, and Holland, which fail to highlight the differences between ADELI and NDE as significant.

Finally, the Quade test find significant difference between ADELI and MABC, GOTLBO, PSO, ISCA, NNA, CWOA, WW for every post-hoc procedure. In the DE and IJAYA cases, ADELI obtains better results in R_{p1} estimation according Finner post-hoc procedure only. This result supports the conclusion that, although ADELI outperforms the weaker algorithms of our study, its performance differences

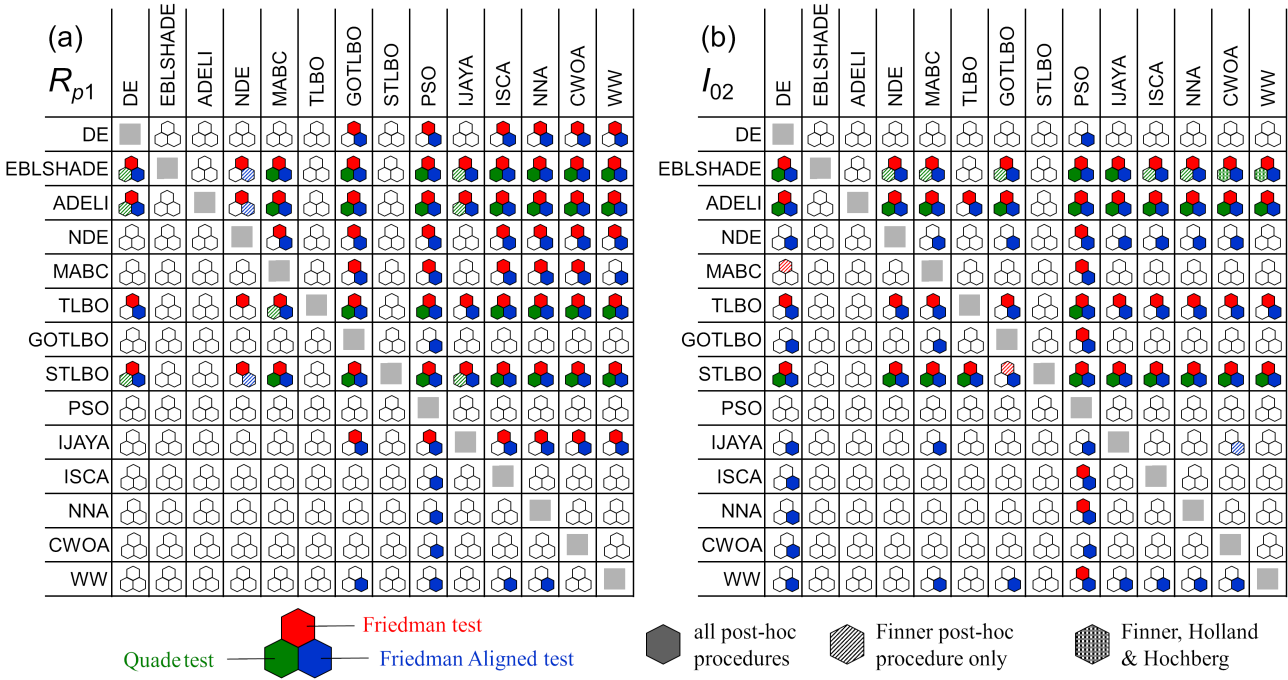


Figure 8: The results of algorithm $1 \times N$ comparisons in R_{p1} (a) and I_{02} (b) estimation by Friedman, Friedman Aligned, and Quade tests in the single-IV case. The colored hexagon indicates that the adjusted p -value, which tests the hypothesis that an algorithm in a row outperforms the algorithm in a column, is not greater than $p_{cr} = 0.1$. The solid fill signifies that every post-hoc procedure resulted in $p < p_{cr}$; the patterned fill indicates that only specific post-hoc procedures achieved this outcome. The correspondence between the color and position of the hexagon to a test as well as the fill pattern to procedures are shown in a legend at the bottom of the figure.

are not significant when compared to other power algorithms (STLBO, EBL SHADE, TLBO).

In our study, a threshold value of $p_{cr} = 0.1$ was adopted to establish a critical level for comparing the effectiveness of two algorithms in both multiple $1 \times N$ and $N \times N$ comparisons. That is, it was determined that the likelihood of obtaining a result as extreme as the observed one, under the assumption that there is no difference between the two algorithms (null hypothesis), was less than 10%.

The statistical results of the algorithm's effectiveness comparison in the task of R_{p1} estimation are shown in Fig. 8(a). In the figure, the outperforming of an algorithm in a row over the algorithm in the column is indicated by a colored hexagon in the corresponding cell. The white hexagon suggests a strong likelihood of the null hypothesis. In fact, the data in Table 3 were used to create the third row in Fig. 8(a). The panel (b) of figure presents the statistical results for I_{02} estimation. The results of the comparison of algorithms based on the other eight parameters are given in the supplementary materials (figure S2).

The results displayed in Fig. 8 demonstrate a consistent trend across all parameters. Among the compared algorithms, EBL SHADE, ADELI, and STLBO consistently outperform the others in $1 \times N$ multiple comparisons. On the other hand, algorithms such as PSO, ISCA, CWOA, and NNA consistently produce lower-quality results. The main changes observed in nonparametric statistical estimation of

different parameters estimation mainly concern algorithms with moderate effectiveness.

For example, when comparing the accuracy of determining R_{p1} and I_{02} , the IJAYA algorithm performs better in the former case. As evident from Figure 3a, IJAYA outperforms GOTLBO, PSO, ISCA, NNA, CWOA, and WW in the results of Friedman and Friedman Aligned tests for every post-hoc procedure considered. While for I_{02} , IJAYA only outperforms DE, MABC, PSO, and CWOA according to the Friedman test, and in the latter case, only for Finner post-hoc procedure. For DE, the situation is similar in the case of I_{02} compared to R_{p1} . According to the results of the Friedman and Friedman Aligned tests, the algorithm loses its advantage over GOTLBO, SCA, NNA, CWOA, and WW. Additionally, the Friedman test no longer shows the improvement of DE over PSO.

In all cases, the Quade test yields higher adjusted p -values. In particular, in the case of the complex parameter, none of the conducted comparisons exceeded the chosen threshold value of the p -value.

The adjusted p -values obtained from the direct comparisons of EBL SHADE, ADELI, and STLBO do not allow for determining the best algorithm among them. However, for this purpose, the results of this top trio of algorithms can be used, obtained from their comparisons with less efficient optimization methods. Table 4 summarizes count of wins and losses for each algorithm in $1 \times N$ multiple comparisons.

Table 4

The total count of wins and losses for each algorithm in $1 \times N$ multiple comparisons using the Friedman, Friedman Aligned, and Quade tests and Finner, Holm, Hochberg, and Holland post-hoc procedures in single-IV case. The criterion for victory was a adjusted p -value less than 0.1.

Algorithm	Wins / Loses										Total
	task										
	I_{01}	n_1	R_{p1}	I_{02}	n_2	R_{p2}	R_s	I_{ph}	RMSPE	Comp	
DE	24/43	56/34	48/35	4/73	48/43	49/34	49/40	45/35	49/48	16/27	388/412
EBLSHADE	108/0	108/0	107/0	103/0	107/0	104/0	111/2	105/0	109/0	88/0	1050/2
ADELI	122/0	110/0	107/0	128/0	110/0	122/0	119/0	105/0	109/0	61/2	1093/2
NDE	35/19	56/32	56/19	36/49	77/32	23/45	73/32	48/8	83/29	23/20	519/285
MABC	8/61	28/69	44/45	9/57	40/55	4/82	32/51	32/66	44/62	8/30	249/578
TLBO	80/3	102/0	101/0	84/13	99/0	87/18	93/10	94/0	100/0	65/2	905/46
GOTLBO	8/60	12/73	4/84	16/49	20/74	13/54	20/61	4/80	16/85	13/28	126/648
STLBO	109/0	110/0	107/0	125/0	107/0	119/0	116/0	105/0	109/0	81/0	1088/0
PSO	0/84	8/88	0/100	0/108	4/101	0/96	0/124	0/96	20/70	4/49	72/916
IJAYA	28/28	56/34	48/35	13/52	45/43	54/34	20/61	56/29	57/38	16/34	393/388
ISCA	8/56	12/76	4/84	12/45	28/65	16/51	8/61	17/68	0/92	16/32	121/630
NNA	33/29	0/92	4/84	12/49	12/84	12/57	8/77	12/80	0/92	0/52	93/696
CWOA	8/60	0/96	4/80	8/52	8/84	4/83	20/61	0/88	0/92	0/52	52/748
WW	0/96	12/76	16/76	36/43	0/108	10/60	12/77	12/66	0/92	0/52	98/844

The maximum possible number of wins achieved in every 10 tasks is 156, obtained from comparing with 13 algorithms in 3 tests using 4 procedures. As can be seen, among the compared algorithms, ADELI showed the highest count of statistically confirmed improvements (1093) over others, indicating its superior performance. Conversely, STLBO demonstrated the lowest count of defeats (0) in similar comparisons, suggesting its consistently strong performance.

Previously, we employed procedures that controlled the Family-Wise Error Rate (FWER) for comparisons with a control algorithm. We tested each of the 14 algorithms individually to determine if any of them were superior to the others. Below are the results of the carried out a multiple comparisons in which all possible pairwise comparisons need to be computed ($N \times N$ comparison), and three procedures (Shaffer's static, Nemenyi, and Holm) have been used to control FWER. These procedures take into account that the hypotheses being tested belonging to a family of all pairwise comparisons are logically interrelated; thus not all combinations of true and false hypotheses are possible.

Starting from the analysis performed by the Friedman test over our results, we can raise the 91 hypotheses of equality among the 14 algorithms of our study for each task, and apply the methods mentioned earlier to contrast them. Table 5 lists the part of the hypotheses and the adjusted p -values achieved on the task of I_{01} estimation. For the remaining 46 hypotheses not indicated in the table, a p -value of 1 was obtained after applying each of the procedures. The full version of the table as well as the data, obtained for other task, are given in the supplementary material (tables S144-S153).

It can be seen that using a level of significance 0.1, only 37 hypotheses of equality are rejected by the Nemenyi, Holm, and Shaffer methods. These hypotheses show the improvement of EBL SHADE, ADELI, TLBO, and STLBO

over DE, NDE, MABC, GOTLBO, PSO, ISCA, NNA, CWOA, and WW, and NNA over WW. None of the remaining 54 hypotheses can be rejected using these procedures.

It should be noted that when testing complementary hypotheses ("algorithm A vs algorithm B" and "algorithm B vs algorithm A"), only in one out of the two cases can a p -value less than 1 be obtained. For instance, when using the Nemenyi procedure to task I_{01} evaluating of comparing "ADELI vs MABC" a p -value of $5.84 \cdot 10^{-9}$ was obtained. Conversely, when comparing "MABC vs ADELI", the p -value was 1. The p -values were computed for all possible hypotheses in the study to identify algorithms whose results statistically deviate from those of other algorithms. In this case, a critical value of $p_{cr} = 0.1$ was used, similar to the $1 \times N$ multiple comparisons. Typical examples of the obtained results for specific parameter cases are presented in Fig. 9. For more comprehensive data, please refer to figure S3 in the supplementary materials. Generalized results regarding the total count of victories and defeats in the $N \times N$ comparisons are listed in Table 6. In the case of $N \times N$ comparisons, the maximum possible number of wins achieved in every 10 tasks is 39, obtained from comparing 13 algorithms in 3 post-hoc procedures.

In the majority of cases, all post-hoc procedures considered lead to similar conclusions regarding the outperforming of one algorithm over another. For example, in the case of the R_{p1} estimation task, the Nemenyi procedure disagrees with Holm and Shaffer methods in only 4 out of 57 cases. Specifically, this occurs for the hypotheses "DE vs WW," "MABC vs ISCA," "MABC vs NNA," and "TLBO vs NDE"—see Fig. 9(a). On the other hand, as evident from Fig. 9(b), such situations are not observed at all for the I_{02} task. The Holm procedure results, in general, differs from the Shaffer procedure ones in only two comparisons: the improvement

Table 5

Adjusted p -values for tests for $N \times N$ multiple comparisons of I_{01} estimation among all methods in the single-IV case ($p < 1.0$ are only shown).

Hypothesis	Nemenyi	post-hoc procedure Holm	Shaffer
ADELI versus WW	<1E-13	<1E-13	<1E-13
ADELI versus NDE	1.17195E-12	1.15907E-12	1.00453E-12
STLBO versus CWOA	1.17195E-12	1.15907E-12	1.00453E-12
TLBO versus PSO	1.21236E-12	1.17240E-12	1.03917E-12
STLBO versus GOTLBO	1.21236E-12	1.17240E-12	1.03917E-12
ADELI versus DE	1.73772E-12	1.64224E-12	1.48948E-12
STLBO versus DE	1.83875E-12	1.71752E-12	1.57607E-12
ADELI versus CWOA	3.83915E-12	3.50164E-12	3.29070E-12
EBLSHADE versus GOTLBO	4.20286E-12	3.78719E-12	3.60245E-12
STLBO versus NDE	5.01110E-12	4.46043E-12	4.29523E-12
ADELI versus GOTLBO	5.41522E-12	4.76064E-12	4.64162E-12
EBLSHADE versus CWOA	5.98099E-12	5.19229E-12	5.12657E-12
EBLSHADE versus ISCA	1.17195E-11	1.00453E-11	1.00453E-11
EBLSHADE versus DE	1.45282E-11	1.22931E-11	1.06966E-11
EBLSHADE versus NDE	4.17053E-11	3.43725E-11	3.07061E-11
STLBO versus ISCA	8.17133E-11	6.64482E-11	6.01625E-11
TLBO versus WW	8.82197E-11	7.07696E-11	6.49529E-11
TLBO versus MABC	1.07900E-10	8.53717E-11	7.94431E-11
EBLSHADE versus MABC	3.09961E-10	2.38431E-10	2.28213E-10
ADELI versus NNA	3.24570E-10	2.46102E-10	2.38969E-10
ADELI versus ISCA	3.83410E-10	2.86504E-10	2.82291E-10
STLBO versus MABC	1.58351E-09	1.16588E-09	1.16588E-09
STLBO versus NNA	1.83408E-09	1.33021E-09	1.33021E-09
TLBO versus ISCA	3.49326E-09	2.49519E-09	2.22648E-09
ADELI versus MABC	5.83612E-09	4.10452E-09	3.71972E-09
EBLSHADE versus NNA	1.23520E-08	8.55140E-09	7.87272E-09
EBLSHADE versus PSO	1.47150E-08	1.00256E-08	9.37877E-09
STLBO versus PSO	5.32586E-08	3.57008E-08	3.39450E-08
ADELI versus PSO	1.50038E-07	9.89261E-08	.56286E-08
TLBO versus GOTLBO	2.16253E-07	1.40208E-07	1.37831E-07
EBLSHADE versus WW	2.39169E-07	1.52438E-07	1.52438E-07
TLBO versus CWOA	2.89034E-07	1.81043E-07	1.77867E-07
TLBO versus DE	5.91345E-07	3.63905E-07	3.63905E-07
STLBO versus WW	6.86296E-07	4.14794E-07	4.14794E-07
TLBO versus NDE	1.37158E-06	8.13904E-07	7.68687E-07
TLBO versus NNA	1.17758E-04	6.72904E-05	6.59964E-05
NNA versus WW	2.21281E-02	1.24015E-02	1.24015E-02
IJAYA versus WW	2.36193E-01	1.29777E-01	1.24585E-01
NNA versus PSO	2.36193E-01	1.29777E-01	1.24585E-01
NDE versus WW	4.04596E-01	2.13413E-01	2.13413E-01
DE versus WW	6.28685E-01	3.24706E-01	3.24706E-01
CWOA versus WW	8.94683E-01	4.52257E-01	4.52257E-01
GOTLBO versus WW	1.0	5.07626E-01	5.07626E-01
IJAYA versus PSO	1.0	8.15876E-01	7.97333E-01
NNA versus MABC	1.0	9.64793E-01	9.64793E-01

of IJAYA over GOTLBO in the n_1 estimation and the outperforming of TLBO over NNA for the composite parameter.

Totally $1 \times N$ multiple comparisons exhibit more powerful behavior than $N \times N$ ones, reaching the lower p -values. As a result, IJAYA did not lose in any of the $N \times N$ comparisons — see Table 6. Another striking example

can be observed when considering the case of the composite parameter. Based on the $1 \times N$ comparisons, conclusions were drawn about the outperforming of one algorithm over another in 67 cases, whereas for the $N \times N$ comparisons, such situations were found in only 20 cases: the improvement of EBLSHADE over MABC, GOTLBO, PSO, ISCA, NNA, CWOA, and WW, the statistically significant difference ADELI and GOTLBO, PSO, NNA, CWOA,

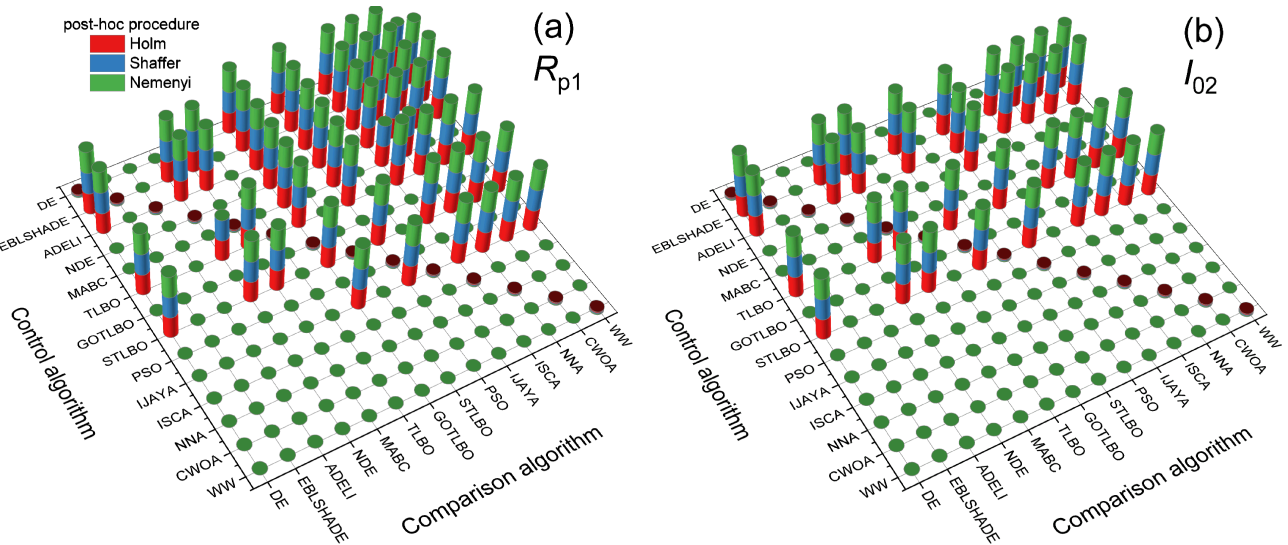


Figure 9: The results of $N \times N$ multiple comparisons of R_{p1} (a) and I_{02} (b) estimation among all algorithms in the single-IV case. The colored cylinder indicates that the adjusted p -value, which tests the control algorithm outperforms the comparison algorithm, is not greater than $p_{lim} = 0.1$. The correspondence between the color of the cylinder to a post-hoc procedure is shown in the figure's legend.

Table 6

The total count of wins and losses for each algorithm in $N \times N$ multiple comparisons using the Friedman test and Shaffer's static, Nemenyi, and Holm post-hoc procedures in single-IV case. The criterion for victory was a adjusted p -value less than 0.1.

Algorithm	Wins / Loses										Total
	I_{01}	n_1	R_{p1}	I_{02}	n_2	R_{p2}	R_s	I_{ph}	RMSPE	Comp	
DE	0/12	17/12	17/12	0/12	12/12	14/12	5/12	17/12	15/15	0/0	97/111
EBLSHADE	27/0	27/0	27/0	27/0	27/0	27/0	27/0	27/0	26/0	21/0	263/0
ADELI	27/0	27/0	27/0	27/0	27/0	27/0	27/0	27/0	27/0	14/0	257/0
NDE	0/12	21/12	18/11	3/12	18/9	3/12	18/11	21/9	24/8	0/0	126/96
MABC	0/12	0/15	10/12	0/12	11/12	0/17	3/12	2/15	12/15	0/3	38/125
TLBO	27/0	27/0	26/0	27/0	24/0	27/0	26/0	24/0	24/0	10/0	242/0
GOTLBO	0/12	0/18	0/24	0/12	3/15	0/12	3/15	0/21	0/21	0/5	6/155
STLBO	27/0	27/0	27/0	27/0	27/0	27/0	27/0	27/0	27/0	11/0	254/0
PSO	0/12	0/21	0/24	0/15	0/24	0/21	0/34	0/23	0/18	0/12	0/204
IJAYA	0/0	16/0	18/0	0/0	12/0	11/0	3/0	18/0	18/0	0/0	96/0
ISCA	0/12	0/21	0/23	0/12	3/15	0/12	2/15	0/21	0/24	0/3	5/158
NNA	3/12	0/21	0/23	0/12	0/23	0/14	0/17	0/21	0/24	0/9	3/176
CWOA	0/12	0/21	0/21	0/12	0/24	0/18	3/15	0/21	0/24	0/12	3/180
WW	0/15	0/21	0/20	0/12	0/30	0/18	2/15	0/20	0/24	0/12	2/187

and WW, and outperforming of both TLBO and STLBO over PSO, NNA, CWOA, and WW. Consequently, $N \times N$ comparisons provide a less precise ranking of all algorithms. However, it is still possible to identify the best and worst-performing algorithms. The obtained data reveal that EBL SHADE, ADELI, and STLBO are the top-performing algorithms in all tasks, while PSO, ISCA, NNA, CWOA, and WW are the worst-performing.

Thus, the results presented in this subsection demonstrate that among the examined algorithms, none can be applied for the maximally accurate determination of a specific individual parameter (e.g., only R_{p2} or only I_{02}) in the opposed two-diode model. The algorithms that exhibit

high efficiency (EBLSHADE, ADELI, and STLBO) allow for the most precise estimation of all parameters. However, certain algorithms really display higher accuracy in determining specific parameters. Indeed, DE and IJAYA are the most effective in estimating R_{p2} and I_{ph} — see table S1. Nevertheless, this highest level of accuracy appears unworthy of significant attention when compared to other optimization methods. As a result, the performance metrics of algorithms for individual parameters will not be analyzed in the following subsection, dedicated to the analysis of IV curves with different parameter ratios.

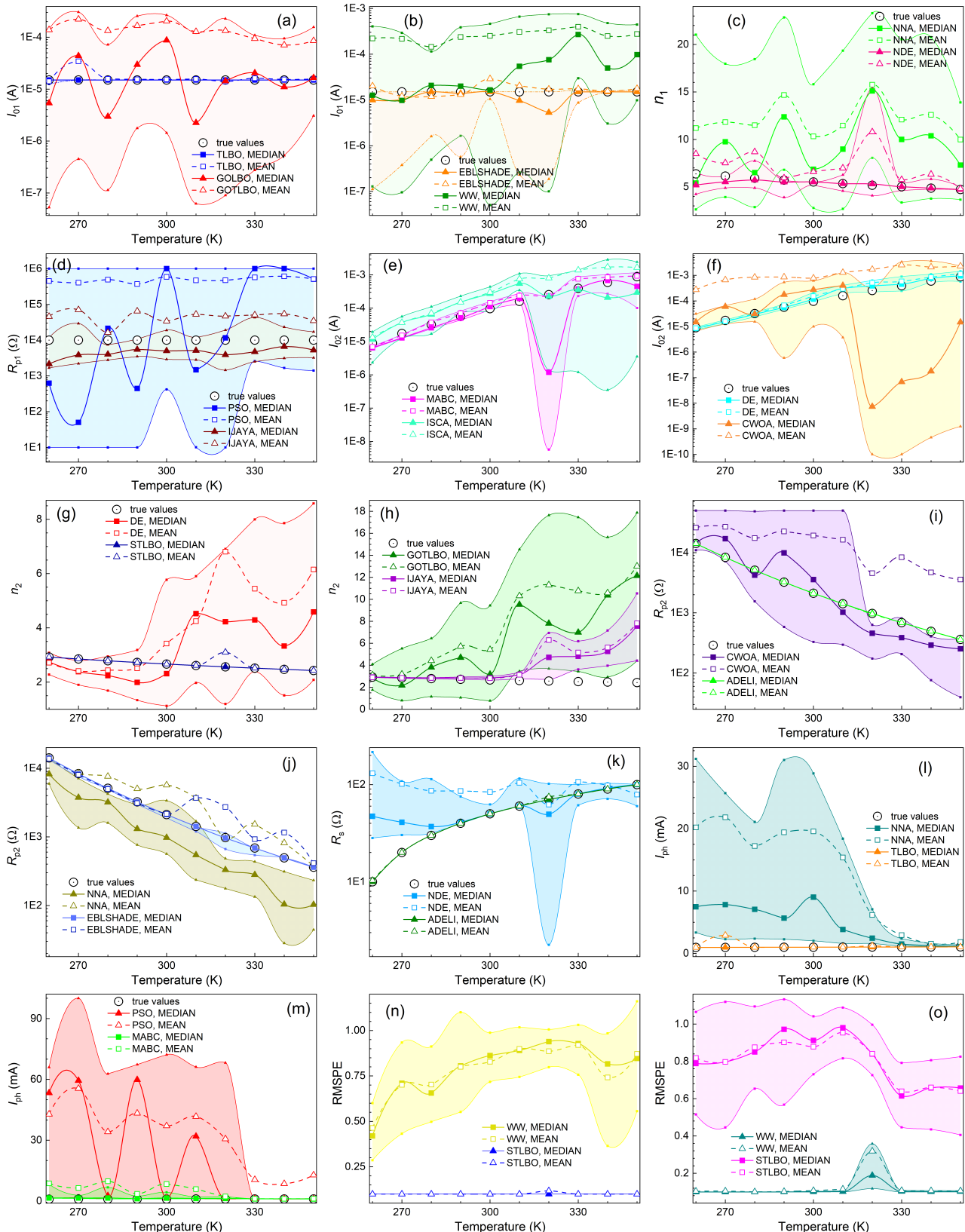


Figure 10: Dependences of the I_{01} (a, b), n_1 (c), R_{p1} (d), I_{02} (e, f), n_2 (g, h), R_{p2} (i, j), R_s (k), I_{ph} (l, m), and RMSPE (n, o) estimation by different algorithm on the synthesis temperature. The IV-set is used. The circles represent the values, which have been used in IV curve simulations, the filled marks represent the median values, and the empty marks represent the mean values. The colored regions correspond to the IQR. The lines only serve as guide to the eye.

Table 7

The results of Wilcoxon signed-rank test with a level of significance $\alpha = 0.05$ in the IV-set case. The “+” indicated that the null hypothesis was rejected, and the control algorithm (in the row) performed better than the comparison algorithm (in the column). The “0” indicates to rejection of the hypothesis about outperforming the control algorithm.

Control algorithm	Comparison algorithm												Total		
	DE	EBLSHADE	ADELI	NDE	MABC	TLBO	GOTLBO	STLBO	PSO	IJAYA	ISCA	NNA	CWOA	WW	(+/-/-/+)
DE	■	0	0	0	+	0	+	0	+	0	+	+	+	+	7/0/6
EBLSHADE	+	■	0	+	+	0	+	0	+	+	+	+	+	+	10/0/3
ADELI	+	+	■	+	+	+	+	+	+	+	+	+	+	+	13/0/0
NDE	+	0	0	■	+	0	+	0	+	+	+	+	+	+	9/0/4
MABC	0	0	0	0	■	0	+	0	+	0	+	+	+	+	6/0/7
TLBO	+	+	0	+	+	■	+	0	+	+	+	+	+	+	11/1/1
GOTLBO	0	0	0	0	0	0	■	0	+	0	+	+	+	+	5/0/8
STLBO	+	+	0	+	+	0	+	■	+	+	+	+	+	+	11/1/1
PSO	0	0	0	0	0	0	0	0	■	0	0	0	0	0	0/4/9
IJAYA	+	0	0	0	+	0	+	0	+	■	+	+	+	+	8/0/5
ISCA	0	0	0	0	0	0	0	0	0	0	■	0	0	0	0/3/10
NNA	0	0	0	0	0	0	0	0	0	0	0	■	0	0	0/3/10
CWOA	0	0	0	0	0	0	0	0	0	0	0	0	■	0	0/4/9
WW	0	0	0	0	0	0	0	0	0	0	0	+	0	■	1/3/9

3.3.2. Evaluation of IV-set

Fig. 3 shows several typical fitting results of a set of synthetic IV curves simulated according to the opposed two-diode model using the parameter values described in Sec. 2.2.2. A more comprehensive and enhanced version, including the fitting results obtained using each algorithm, is provided in the supplementary materials (figure S4). Similar to the single-IV case, the algorithms EBLSHADE, ADELI, NDE, IJAYA, TLBO, and STLBO show the highest agreement between the fitting curves and the points of synthesized current-voltage curves. Fig. 10 represents a portion of the results obtained from evaluating solar cell parameters using various algorithms, along with the corresponding RMSPE data. The supplementary material provides the dependencies of all parameters on synthesis temperature as determined by all the algorithms — see figures S5-S13. The results in terms of MEAN, MEDIAN, STD, and IQR are tabulated as well (table S154 in the supplementary material).

It should be noted that in several cases, the accuracy of parameter estimation depends on temperature, even for constant parameters. For instance, as the temperature increases, the errors in determining R_{p1} by NDE, MABC, GOTLBO, IJAYA, ISCA, and WW decrease. However, under the same conditions, the estimation quality of I_{01} using DE, ISCA, and WW worsens. These results indicate that the accuracy of parameter estimation depends not only on the parameter value itself but also on its ratio with other parameters. A comprehensive investigation into the specific dependencies of parameter estimation accuracy for each algorithm has not been conducted. This study aimed to determine the best algorithms rather than elucidate the peculiarities of their application in the context of opposed the two-diode model.

The presented data display several characteristics that were also observed in the single-IV case. For instance, the error in parameters estimating by mean values is higher

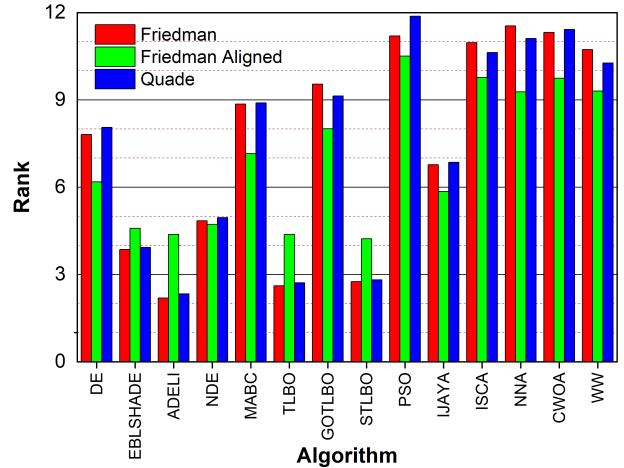


Figure 11: Ranking of the algorithms according to Friedman, Friedman Aligned, and Quade tests in the IV-set case.

compared to that of median values in the majority of cases. Exceptions are observed at some temperatures only when evaluating I_{01} using IJAYA, n_1 using IJAYA and DE, R_{p1} using DE and MABC, and R_s using DE and WW. However, for high-precision algorithms, the deviation of MEDIAN from the true value does not exceed the deviation of MEAN. Additionally, these algorithms exhibit small IQR values that do not exceed STD. Similar to the previous case, small RMSPE values do not always indicate high accuracy in determining the parameters of a solar cell.

At the same time, the number of algorithms exhibiting minimal errors has decreased. Significant deviations from true values are observed for median values of I_{01} , n_1 , R_{p1} , n_2 , R_s , and I_{ph} evaluated by EBLSHADE at various temperatures, as well as for median values of diode D1 characteristics and series resistor determined using TLBO at

260 K. Thus, only ADELI and STLBO remain as algorithms without visible errors. Although this claim of infallibility applies only to median values, substantial errors are observed for mean values in several cases. Simultaneously, EBL SHADE, TLBO, IJAYA, and NDE form a group of algorithms with low RMSPE values but imperfect model parameter estimation.

In the IV-set case, to assess the statistical performance of compared algorithms, the run time and all APE_{MEDIAN} and RMSPE_{MEDIAN} for each IV curve were taken into account. This approach is similar to the use of the Comp parameter in the previous subsection; however, in this scenario, $N_{pr} = 81$ is employed:

$$N_{pr} = 10 T_{\text{values}} \times (8 \text{APE}_{\text{MEDIAN}} + 1 \text{RMSPE}_{\text{MEDIAN}}) + 1 t_{\text{run}} .$$

Therefore, such an approach is well-suited for nonparametric statistical analysis of $k = 14$ meta-heuristic algorithms. Certainly, at first sight, it would be interesting to consider incorporating an additional 80 values of the interquartile range into the dataset. This approach could provide consideration into the stability of algorithm performance as well. However, it is known [76] that for multiple comparisons, a value of $N_{pr} \geq 8 \cdot k = 112$ could be too high, obtaining no significant comparisons as a result.

Table 7 gives the statistical results produced by the Wilcoxon sign–rank test. As the table states, ADELI outperforms all other algorithms with a level of significance $\alpha = 0.05$. STLBO and TLBO show an improvement over DE, EBL SHADE, NDE, MABC, GOTLBO, PSO, IJAYA, ISCA, NNA, CWOA, and WW. The counts of statistical significant cases (+/-) are presented in the last row of Table 7. It can be seen than PSO, ISCA, NNA, and CWOA did not outperform any of the algorithms, whereas WW statistically significantly improved over NNA only. Therefore, although these algorithms have promising run times, they are not recommended for parameter estimation of a solar cell based on the opposed two-diode model.

The p -values required to test the null hypothesis, computed using the Friedman, Friedman Aligned, Quade tests, and the Iman–Davenport extension, can be found in table S2 of the supplementary materials. None of these values exceeds $2.3 \cdot 10^{-6}$, thereby rejecting the hypothesis of equivalent medians in all tests.

Ranks achieved by the Friedman, Friedman Aligned, and Quade tests are shown in Fig. 11 and table S3 in the supplementary material. As per the given results, ADELI has been placed at first rank by Friedman and Quade tests, and STLBO has ranked first by the Friedman Aligned test. TLBO has been recorded as second-best algorithm by all three tests. Furthermore, PSO was recognized as the worst-performing algorithm by the tests' unanimous decision.

The p -values, obtained for $1 \times N$ multiple comparisons are shown in tables S155–168 in the supplementary material. There are results of applying Finner, Holm, Hochberg, and Holland procedures, as a post-hoc method after Friedman, Friedman Aligned, and Quade tests. The reader is referred to

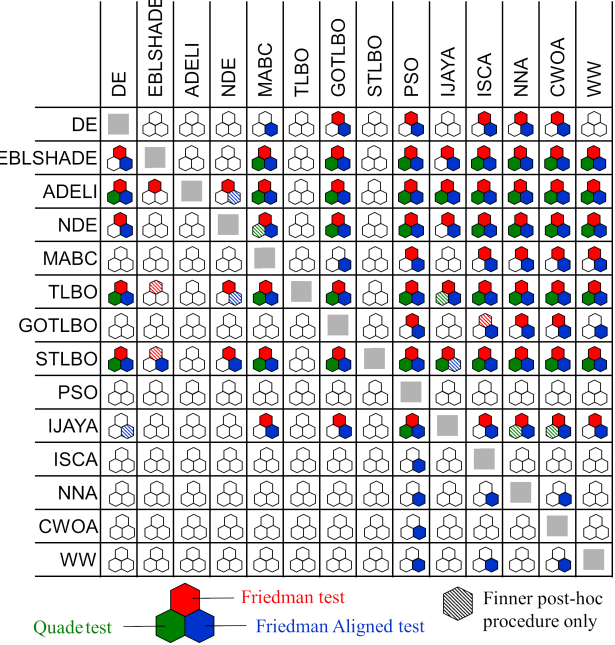


Figure 12: The results of algorithm $1 \times N$ comparisons by Friedman, Friedman Aligned, and Quade tests in the IV-set case. The colored hexagon indicates that the adjusted p -value, which tests the hypothesis that an algorithm in a row outperforms the algorithm in a column, is not greater than $p_{cr} = 0.1$. The solid fill signifies that every post-hoc procedure resulted in $p < p_{cr}$; the dashed fill indicates that the Finner post-hoc procedure was the only method that produced this result. The correspondence between the color and position of the hexagon to a test is shown in a legend at the bottom of the figure.

supplementary material (table S169) for p -values of applying Shaffer, Nemenyi, and Holm post-hoc procedures after the Friedman test in the case of $N \times N$ multiple comparisons. The results, which determine whether one algorithm yielded a statistically better estimation of parameters than the other (with a p -value $\leq p_{cr} = 0.1$), are summarized in Fig. 12 and 13 for $1 \times N$ and $N \times N$ comparisons, respectively. The counts of statistically significant cases are presented in the Table 8.

As can be seen, ADELI, TLBO, and STLBO were never outperformed by any of the algorithms, both in the case of $1 \times N$ and $N \times N$ multiple comparisons. By the way, for $N \times N$ comparisons, the same property is observed with EBL SHADE and IJAYA. Overall, the parameter estimation results obtained from the set of IV curves using ADELI, TLBO, and STLBO algorithms for $N \times N$ comparisons in the opposed two-diode model are practically indistinguishable (when it comes to precise p -values, only minor differences can be observed). In $1 \times N$ comparisons, TLBO demonstrates lower performance compared to ADELI and STLBO, in terms of efficiency when compared to the EBL SHADE algorithm. Specifically, the improvement of TLBO over EBL SHADE is proved only by the Finner procedure applied in the Friedman test. Based on $1 \times N$ comparisons, it is

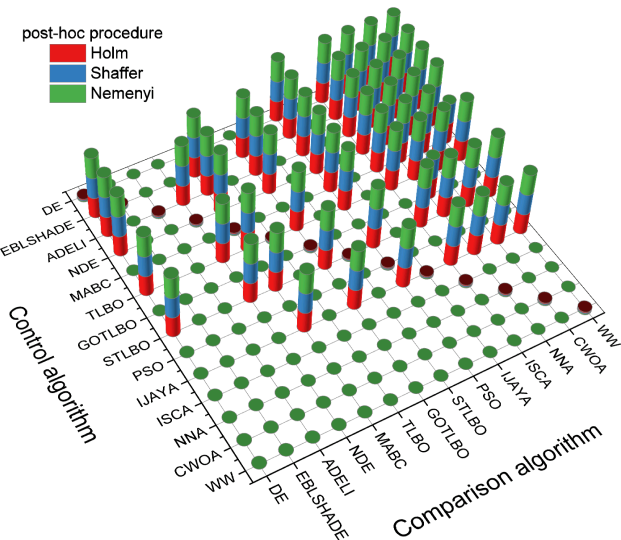


Figure 13: The results of multiple comparisons among all algorithms in the IV-set case. The colored cylinder indicates that the adjusted p -value, which tests the control algorithm outperforms the comparison algorithm, is not greater than $p_{cr} = 0.1$. The correspondence between the color of the cylinder to a post-hoc procedure is shown in the figure's legend.

Table 8

The total count of wins and losses for each algorithm in $1 \times N$ and $N \times N$ multiple comparisons using the all tests and post-hoc procedures in the IV-set case. The criterion for victory was a adjusted p -value less than 0.1. The best results are bolded.

Algorithm	Wins / Losses	
	$1 \times N$ comparisons	$N \times N$ comparisons
DE	44/53	15/15
EBLSHADE	100/6	24/0
ADELI	117/0	27/0
NDE	97/18	24/9
MABC	44/69	14/18
TLBO	111/0	27/0
GOTLBO	25/80	2/18
STLBO	118/0	27/0
PSO	0/112	0/24
IJAYA	63/46	21/0
ISCA	4/97	0/24
NNA	12/93	0/26
CWOA	4/101	0/24
WW	12/80	0/23

observed as well that there are slight differences between ADELI and STLBO, primarily when compared to the non-worst algorithms. For instance, the Quade test confirms the improvement of ADELI over EBL SHADE for every post-hoc procedure, however, the Friedman and Friedman Aligned tests did not show statistically significant differences between these algorithms. Meanwhile, the Friedman Aligned and Quade tests find a difference between STLBO and EBL SHADE for every post-hoc procedure and Finner procedure only, respectively. Regarding comparison with

NDE, the Friedman Aligned test demonstrated that STLBO is better according to all post-hoc procedures. In contrast, for ADELI, this outperforming was only observed using the Finner method. In the case of IJAYA, the results of the Friedman Aligned test show a reversal: only the Finner procedure indicates an improvement for STLBO, whereas ADELI outperforms all post-hoc methods utilized.

In deciding the optimal algorithm for parameter estimation of solar cell parameters from the IV curve using the opposed two-diode model, the practical choices boil down to EBL SHADE, ADELI, TLBO, and STLBO. However, TLBO exhibited lower performance when applied in the single-IV case. The parameter estimation error when using EBL SHADE was not always minimal in the IV-set case. Despite the minimal advantage in terms of win counts in $1 \times N$ comparisons (see Table 8), we hesitate to declare STLBO as the best. In our opinion, STLBO and ADELI both hold the top position in the competition conducted in this study.

4. Conclusion

In this paper, the possibility of using a meta-heuristic algorithms to solve the parameter estimation problems of photovoltaic cells with S-shaped current-voltage characteristics has been explored. The parameter estimation has been performed within the framework of the opposed two-diode model. A total of 16 meta-heuristic algorithms from various classes were implemented to extract the solar cell parameters from synthetic IV curves, which were generated with a range of parameter values. The obtained results have been compared using nonparametric statistical procedures, including pairwise comparisons, $1 \times N$ multiple comparisons, and $N \times N$ multiple comparisons.

Research has demonstrated that utilizing a squared error-based fitness function offers clear advantages in tackling a provided problem. The overall performance results of various algorithms generally fit the No Free Lunch theory. GOTLBO, PSO, ISCA, NNA, CWOA, and WW are completely unsuitable for parameter estimation according to the opposed two-diode model. The results of DE, NDE, MABC, and IJAYA are not as poor as those in the previous group; however, in general, it is still not recommended to use these algorithms for solving parameter identification problems. Generally, the EBL SHADE and TLBO are effective in accurately determining parameter values in most cases. However, investigation has shown that these algorithms may make mistakes under certain conditions. Therefore, EBL SHADE and TLBO applications in the case of solar cells with S-shaped IV curves should be approached with caution. Finally, results have illustrated that STLBO and ADELI have superior performance in terms of accuracy and reliability when compared with other used algorithms. In particular, these two algorithms successfully solve the task of accurately determining parameters from similar IV curves corresponding to photovoltaic cells with distinct characteristics.

It is important to note that in this study, the parameters were obtained from idealized IV curves, where the voltage-current relationships were precisely defined by Eq. (2). In a real experiment, there is a potential for errors in the measurement of both current and voltage. Hence, it would be worthwhile to explore the efficacy of various meta-heuristic algorithms in determining parameters from IV data corrupted by noise in future research.

This work of test and comparative analysis of different meta-heuristic algorithms for determination of solar cell parameters should be useful for further research and development on photovoltaic systems.

References

- [1] A. Divya, T. Adish, P. Kaustubh, P. Zade, Review on recycling of solar modules/panels, *Sol. Energ. Mat. Sol.* 253 (2023) 112151.
- [2] X. Wang, X. Tian, X. Chen, L. Ren, C. Geng, A review of end-of-life crystalline silicon solar photovoltaic panel recycling technology, *Sol. Energ. Mat. Sol.* 248 (2022) 111976.
- [3] E. Sesa, D. Darwis, X. Zhou, W. J. Belcher, P. C. Dastoor, Experimental determination of the relationship between the elements of a back-to-back diode model for organic photovoltaic cells' S-shaped I-V characteristics and cell structure, *AIP Adv.* 9 (2019) 025014.
- [4] B. Y. Finck, B. J. Schwartz, Understanding the origin of the S-curve in conjugated polymer/fullerene photovoltaics from drift-diffusion simulations, *Appl. Phys. Lett.* 103 (2013) 053306.
- [5] L. Zuo, J. Yao, H. Li, H. Chen, Assessing the origin of the S-shaped I-V curve in organic solar cells: An improved equivalent circuit model, *Sol. Energ. Mat. Sol.* 122 (2014) 88–93.
- [6] F. A. de Castro, J. Heier, F. A. Nüesch, R. Hany, Origin of the kink in current-density versus voltage curves and efficiency enhancement of polymer-C₆₀ heterojunction solar cells, *IEEE J. Sel. Top. Quantum Electron.* 16 (2010) 1690–1699.
- [7] B. Romero, G. del Pozo, B. Arredondo, D. Martín-Martín, M. P. R. Gordo, A. Pickering, A. Pérez-Rodríguez, E. Barrena, F. J. García-Sánchez, S-shaped I – V characteristics of organic solar cells: Solving mazhari's lumped-parameter equivalent circuit model, *IEEE Trans. Electron Devices* 64 (2017) 4622–4627.
- [8] J. Gao, J. M. Luther, O. E. Semonin, R. J. Ellingson, A. J. Nozik, M. C. Beard, Quantom dot size dependent J-V characteristics in heterojunction ZnO/PbS quantum dot solar cells, *Nano Lett.* 11 (2011) 1002–1008.
- [9] R. Saive, S-shaped current–voltage characteristics in solar cells: A review, *IEEE J. Photovolt.* 9 (2019) 1477–1484.
- [10] P. J. Roland, K. P. Bhandari, R. J. Ellingson, Electronic circuit model for evaluating S-kink distorted current-voltage curves, in: 2016 IEEE 43rd Photovoltaic Specialists Conference (PVSC), pp. 3091–3094.
- [11] A. Gaur, P. Kumar, An improved circuit model for polymer solar cells, *Prog. Photovoltaics Res. Appl.* 22 (2014) 937–948.
- [12] V.-H. Tran, R. B. Ambade, S. B. Ambade, S.-H. Lee, I.-H. Lee, Low-temperature solution-processed sno₂ nanoparticles as a cathode buffer layer for inverted organic solar cells, *ACS Appl Mater Interfaces* 9 (2017) 1645–1653.
- [13] G. Lastra, V. S. Balderrama, L. Reséndiz, J. Pallarès, L. F. Marsal, V. Cabrera, M. Estrada, Air environment degradation of a high-performance inverted ptb7-th:pc70bm solar cell, *IEEE J. Photovolt.* 9 (2019) 464–468.
- [14] F. Xu, J. Zhu, R. Cao, S. Ge, W. Wang, H. Xu, R. Xu, Y. Wu, M. Gao, Z. Ma, F. Hong, Z. Jiang, Elucidating the evolution of the current-voltage characteristics of planar organometal halide perovskite solar cells to an S-shape at low temperature, *Sol. Energ. Mat. Sol.* 157 (2016) 981–988.
- [15] F. Yu, G. Huang, W. Lin, C. Xu, W. Deng, X. Ma, J. Huang, Lumped-parameter equivalent circuit modeling of solar cells with S-shaped i-v characteristics, *Solid-State Electron.* 156 (2019) 79–86.
- [16] E. Veinberg-Vidal, C. Dupré, P. Garcia-Linares, C. Jany, R. Thibon, T. Card, T. Salvetat, P. Scheiblin, C. Brughera, F. Fournel, Y. Desieres, Y. Veschetti, V. Sanzone, P. Mur, J. Decobert, A. Datas, Manufacturing and characterization of iii-v on silicon multijunction solar cells, *Energy Procedia* 92 (2016) 242–247.
- [17] B. Mazhari, An improved solar cell circuit model for organic solar cells, *Sol. Energ. Mat. Sol.* 90 (2006) 1021–1033.
- [18] F. Yu, G. Huang, W. Lin, C. Xu, An analysis for S-shaped I-V characteristics of organic solar cells using lumped-parameter equivalent circuit model, *Sol. Energy* 177 (2019) 229–240.
- [19] F. J. García-Sánchez, B. Romero, Equivalent circuit models for next generation photovoltaic devices with S-shaped I-V curves, in: 2019 8th International Symposium on Next Generation Electronics (ISNE), pp. 1–4.
- [20] F. J. García-Sánchez, D. Lugo-Muñoz, J. Muci, A. Ortiz-Conde, Lumped parameter modeling of organic solar cells' S-shaped I-V characteristics, *IEEE J. Photovolt.* 3 (2013) 330–335.
- [21] F. De Castro, A. Laudani, F. Riganti Fulginei, A. Salvini, An in-depth analysis of the modelling of organic solar cells using multiple-diode circuits, *Sol. Energy* 135 (2016) 590–597.
- [22] F. J. García-Sánchez, B. Romero, D. Lugo-Muñoz, G. del Pozo, B. Arredondo, J. J. Liou, A. Ortiz-Conde, Modelling solar cell S-shaped IV characteristics with dc lumped-parameter equivalent circuit - a review, *Facta universitatis. Series electronics and energetics* 30 (2017) 327–350.
- [23] D. Wolpert, W. Macready, No free lunch theorems for optimization, *IEEE Trans. Evol. Comput.* 1 (1997) 67–82.
- [24] D. H. Muhsen, A. B. Ghazali, T. Khatib, I. A. Abed, A comparative study of evolutionary algorithms and adapting control parameters for estimating the parameters of a single-diode photovoltaic module's model, *Renew. Energ.* 96 (2016) 377–389.
- [25] R. Abbassi, A. Abbassi, A. A. Heidari, S. Mirjalili, An efficient salp swarm-inspired algorithm for parameters identification of photovoltaic cell models, *Energy Convers. Manage.* 179 (2019) 362–372.
- [26] T. Sudhakar Babu, J. Prasanth Ram, K. Sangeetha, A. Laudani, N. Rajasekar, Parameter extraction of two diode solar PV model using fireworks algorithm, *Sol. Energy* 140 (2016) 265–276.
- [27] H. M. Ridha, H. Hizam, C. Gomes, A. A. Heidari, H. Chen, M. Ahmadipour, D. H. Muhsen, M. Alghrairi, Parameters extraction of three diode photovoltaic models using boosted LSHADE algorithm and Newton Raphson method, *Energy* 224 (2021) 120136.
- [28] Q. Niu, L. Zhang, K. Li, A biogeography-based optimization algorithm with mutation strategies for model parameter estimation of solar and fuel cells, *Energy Convers. Manage.* 86 (2014) 1173–1185.
- [29] L. Guo, Z. Meng, Y. Sun, L. Wang, Parameter identification and sensitivity analysis of solar cell models with cat swarm optimization algorithm, *Energy Convers. Manage.* 108 (2016) 520–528.
- [30] J. P. Ram, T. S. Babu, T. Dragicevic, N. Rajasekar, A new hybrid bee pollinator flower pollination algorithm for solar pv parameter estimation, *Energy Convers. Manage.* 135 (2017) 463–476.
- [31] H. M. Ridha, Parameters extraction of single and double diodes photovoltaic models using Marine Predators Algorithm and Lambert W function, *Sol. Energy* 209 (2020) 674–693.
- [32] M. Abdel-Basset, D. El-Shahat, R. K. Chakrabortty, M. Ryan, Parameter estimation of photovoltaic models using an improved marine predators algorithm, *Energy Convers. Manage.* 227 (2021) 113491.
- [33] H. Chen, S. Jiao, A. A. Heidari, M. Wang, X. Chen, X. Zhao, An opposition-based sine cosine approach with local search for parameter estimation of photovoltaic models, *Energy Convers. Manage.* 195 (2019) 927–942.
- [34] M. Merchaoui, A. Sakly, M. F. Mimouni, Particle swarm optimisation with adaptive mutation strategy for photovoltaic solar cell/module parameter extraction, *Energy Convers. Manage.* 175 (2018) 151–163.
- [35] G. Xiong, J. Zhang, D. Shi, Y. He, Parameter extraction of solar photovoltaic models using an improved whale optimization algorithm, *Energy Convers. Manage.* 174 (2018) 388–405.

- [36] K. Yu, J. Liang, B. Qu, X. Chen, H. Wang, Parameters identification of photovoltaic models using an improved JAYA optimization algorithm, *Energy Convers. Manage.* 150 (2017) 742–753.
- [37] B. Romero, G. del Pozo, B. Arredondo, Exact analytical solution of a two diode circuit model for organic solar cells showing S-shape using Lambert W-functions, *Sol. Energy* 86 (2012) 3026–3029.
- [38] L. Lóczy, Guaranteed- and high-precision evaluation of the Lambert W function, *Appl. Math. Comput.* 433 (2022) 127406.
- [39] K. Roberts, S. R. Valluri, On calculating the current-voltage characteristic of multi-diode models for organic solar cells, 2015.
- [40] K. Tada, Parameter extraction from S-shaped current–voltage characteristics in organic photocell with opposed two-diode model: Effects of ideality factors and series resistance, *Phys. Status Solidi A* 212 (2015) 1731–1734.
- [41] K. Tada, Bayesian estimation of equivalent circuit parameters of photovoltaic cell with S-shaped current–voltage characteristic, *Phys. Status Solidi A* 218 (2021) 2100403.
- [42] S. M. Sze, M. Lee, *Semiconductor Devices: Physics and Technology*, John Wiley & Sons, Inc, New York, third edition, 2012.
- [43] S. Kondratenko, V. Lysenko, Y. V. Gomeniuk, O. Kondratenko, Y. Kozyrev, O. Selyshchev, V. Dzhagan, D. R. T. Zahn, Charge carrier transport, trapping, and recombination in pedot:pss/n-si solar cells, *ACS Appl. Energy Mater.* 2 (2019) 5983–5991.
- [44] M. A. Green, General temperature dependence of solar cell performance and implications for device modelling, *Prog. Photovoltaics Res. Appl.* 11 (2003) 333–340.
- [45] R. Eberle, A. Fell, F. Schindler, J. Shahid, M. C. Schubert, Breakdown of temperature sensitivity of silicon solar cells by simulation input parameters, *Sol. Energ. Mat. Sol.* 219 (2021) 110836.
- [46] H. Ibrahim, N. Anani, Variations of PV module parameters with irradiance and temperature, *Energy Procedia* 134 (2017) 276–285.
- [47] F. Bradaschia, M. C. Cavalcanti, A. J. do Nascimento, E. A. da Silva, G. M. de Souza Azevedo, Parameter identification for PV modules based on an environment-dependent double-diode model, *IEEE J. Photovolt.* 9 (2019) 1388–1397.
- [48] A. H. Tuan Le, R. Basnet, D. Yan, W. Chen, N. Nandakumar, S. Duttagupta, J. P. Seif, Z. Hameiri, Temperature-dependent performance of silicon solar cells with polysilicon passivating contacts, *Sol. Energ. Mat. Sol.* 225 (2021) 111020.
- [49] O. Dupré, R. Vaillon, M. A. Green, Experimental assessment of temperature coefficient theories for silicon solar cells, *IEEE J. Photovolt.* 6 (2016) 56–60.
- [50] Y. Riesen, M. Stuckelberger, F.-J. Haug, C. Ballif, N. Wyrtsch, Temperature dependence of hydrogenated amorphous silicon solar cell performances, *J. Appl. Phys.* 119 (2016) 044505.
- [51] A. Rana, A. Kumar, S. Chand, R. K. Singh, Exploring deep defect state impact on open circuit voltage of conventional and inverted organic solar cells, *J. Appl. Phys.* 124 (2018) 103101.
- [52] M. Braik, A. Hammouri, J. Atwan, M. A. Al-Betar, M. A. Awadallah, White shark optimizer: A novel bio-inspired meta-heuristic algorithm for global optimization problems, *Knowledge-Based Systems* 243 (2022) 108457.
- [53] J.-S. Pan, L.-G. Zhang, R.-B. Wang, V. Snášel, S.-C. Chu, Gannet optimization algorithm : A new metaheuristic algorithm for solving engineering optimization problems, *Math. Comput. Simulation* 202 (2022) 343–373.
- [54] S. Zhao, T. Zhang, S. Ma, M. Chen, Dandelion optimizer: A nature-inspired metaheuristic algorithm for engineering applications, *Eng. Appl. Artif. Intell.* 114 (2022) 105075.
- [55] K. Wang, M. Ye, Parameter determination of Schottky–barrier diode model using differential evolution, *Solid-State Electron.* 53 (2009) 234–240.
- [56] K. Ishaque, Z. Salam, H. Taheri, A. Shamsudin, A critical evaluation of ea computational methods for photovoltaic cell parameter extraction based on two diode model, *Solar Energy* 85 (2011) 1768–1779.
- [57] Q. Huang, K. Zhang, J. Song, Y. Zhang, J. Shi, Adaptive differential evolution with a lagrange interpolation argument algorithm, *Inform. Sci.* 472 (2019) 180–202.
- [58] M. Tian, X. Gao, Differential evolution with neighborhood-based adaptive evolution mechanism for numerical optimization, *Inform. Sci.* 478 (2019) 422–448.
- [59] R. Tanabe, A. S. Fukunaga, Improving the search performance of shade using linear population size reduction, in: 2014 IEEE Congress on Evolutionary Computation (CEC), pp. 1658–1665.
- [60] A. W. Mohamed, A. A. Hadi, K. M. Jamali, Novel mutation strategy for enhancing SHADE and LSHADE algorithms for global numerical optimization, *Swarm Evol. Comput.* 50 (2019) 100455.
- [61] M. Ye, X. Wang, Y. Xu, Parameter extraction of solar cells using particle swarm optimization, *J. Appl. Phys.* 105 (2009) 094502.
- [62] N. Karaboga, S. Kockanat, H. Dogan, The parameter extraction of the thermally annealed schottky barrier diode using the modified artificial bee colony, *Appl. Intell.* 38 (2013) 279–288.
- [63] S. Mirjalili, A. Lewis, The whale optimization algorithm, *Adv. Eng. Software* 95 (2016) 51–67.
- [64] D. Oliva, M. Abd El Aziz, A. Ella Hassani, Parameter estimation of photovoltaic cells using an improved chaotic whale optimization algorithm, *Appl. Energy* 200 (2017) 141–154.
- [65] A. Sadollah, H. Sayyaadi, A. Yadav, A dynamic metaheuristic optimization model inspired by biological nervous systems: Neural network algorithm, *Appl. Soft Comput.* 71 (2018) 747–782.
- [66] S. J. Patel, A. K. Panchal, V. Kheraj, Extraction of solar cell parameters from a single current–voltage characteristic using teaching learning based optimization algorithm, *Applied Energy* 119 (2014) 384–393.
- [67] X. Chen, K. Yu, W. Du, W. Zhao, G. Liu, Parameters identification of solar cell models using generalized oppositional teaching learning based optimization, *Energy* 99 (2016) 170–180.
- [68] Q. Niu, H. Zhang, K. Li, An improved TLBO with elite strategy for parameters identification of PEM fuel cell and solar cell models, *Int. J. Hydrogen Energy* 39 (2014) 3837–3854.
- [69] Y.-J. Zheng, Water wave optimization: A new nature-inspired metaheuristic, *Comput. Oper. Res.* 55 (2015) 1–11.
- [70] R. Rao, Jaya: A simple and new optimization algorithm for solving constrained and unconstrained optimization problems, *International Journal of Industrial Engineering Computations* 7 (2016) 19–34.
- [71] S. Mirjalili, SCA: A sine cosine algorithm for solving optimization problems, *Knowledge-Based Systems* 96 (2016) 120–133.
- [72] W. Long, T. Wu, X. Liang, S. Xu, Solving high-dimensional global optimization problems using an improved sine cosine algorithm, *Expert Syst. Appl.* 123 (2019) 108–126.
- [73] S. Gupta, K. Deep, A hybrid self-adaptive sine cosine algorithm with opposition based learning, *Expert Syst. Appl.* 119 (2019) 210–230.
- [74] P. P. Biswas, P. Suganthan, G. Wu, G. A. Amaralunga, Parameter estimation of solar cells using datasheet information with the application of an adaptive differential evolution algorithm, *Renew. Energ.* 132 (2019) 425–438.
- [75] V. Sahargahi, V. Majidnezhad, S. T. Afshord, Y. Jafari, An intelligent chaotic clonal optimizer, *Appl. Soft Comput.* 115 (2022) 108126.
- [76] J. Derrac, S. García, D. Molina, F. Herrera, A practical tutorial on the use of nonparametric statistical tests as a methodology for comparing evolutionary and swarm intelligence algorithms, *Swarm Evol. Comput.* 1 (2011) 3–18.